

Cartilage-like protein hydrogels engineered via entanglement

<https://doi.org/10.1038/s41586-023-06037-0>

Received: 10 July 2020

Accepted: 31 March 2023

Published online: 21 June 2023

 Check for updates

Linglan Fu^{1,4}, Lan Li^{2,4}, Qingyuan Bian¹, Bin Xue³, Jing Jin², Jiayu Li¹, Yi Cao³, Qing Jiang² & Hongbin Li¹✉

Load-bearing tissues, such as muscle and cartilage, exhibit high elasticity, high toughness and fast recovery, but have different stiffness (with cartilage being significantly stiffer than muscle)^{1–8}. Muscle achieves its toughness through finely controlled forced domain unfolding–refolding in the muscle protein titin, whereas articular cartilage achieves its high stiffness and toughness through an entangled network comprising collagen and proteoglycans. Advancements in protein mechanics and engineering have made it possible to engineer titin-mimetic elastomeric proteins and soft protein biomaterials thereof to mimic the passive elasticity of muscle^{9–11}. However, it is more challenging to engineer highly stiff and tough protein biomaterials to mimic stiff tissues such as cartilage, or develop stiff synthetic matrices for cartilage stem and progenitor cell differentiation¹². Here we report the use of chain entanglements to significantly stiffen protein-based hydrogels without compromising their toughness. By introducing chain entanglements¹³ into the hydrogel network made of folded elastomeric proteins, we are able to engineer highly stiff and tough protein hydrogels, which seamlessly combine mutually incompatible mechanical properties, including high stiffness, high toughness, fast recovery and ultrahigh compressive strength, effectively converting soft protein biomaterials into stiff and tough materials exhibiting mechanical properties close to those of cartilage. Our study provides a general route towards engineering protein-based, stiff and tough biomaterials, which will find applications in biomedical engineering, such as osteochondral defect repair, and material sciences and engineering.

Load-bearing tissues exhibit finely regulated mechanical properties to uniquely suit their biological functions^{1,14}. To mimic these tissues, protein-based hydrogels have been widely explored¹⁵. Protein hydrogels are generally soft, with Young's moduli lower than 100 kPa (refs. 9,16). Current protein hydrogel technologies have had considerable success in achieving mechanical properties mimicking those of soft load-bearing tissues^{15–17}, such as muscle^{9,10,18}. In comparison, cartilage is much stiffer with a Young's modulus on the order of megapascals (0.2 MPa to several megapascals)⁸ and bears both tensile and compressive loads. Cartilage can withstand a load of up to 100 MPa and sustain millions of loading–unloading cycles without much fatigue, and can rapidly recover its deformation after unloading^{17,19}. Articular cartilage realizes this unique combination of mechanical features through an entangled network of collagen fibres and proteoglycans²⁰. As high stiffness, high toughness and fast recovery are often conflicting properties, it is challenging to use current technologies to engineer stiff and tough protein hydrogels to mimic the mechanical properties of cartilage-like stiff tissues.

To engineer highly stiff and tough protein hydrogels, a higher crosslinking density and an efficient microscopic energy dissipation

mechanism are essential. Muscle uses force-induced unfolding–refolding of titin globular domains to effectively dissipate energy upon muscle overstretching, and rapidly recover upon relaxation^{3,21,22}. This mechanism has been successfully used to engineer soft protein hydrogels to mimic the passive elasticity of muscle^{9–11,18}. We reason that if an efficient method can be developed to significantly enhance the stiffness without embrittling such soft protein biomaterials, one should be able to convert soft protein hydrogels into materials with mechanical properties mimicking those of articular cartilage.

Entanglement as a stiffening mechanism

Increasing a network's chemical crosslinking density will not achieve the goal as it will stiffen but simultaneously embrittle the hydrogel. We resorted to a physical mechanism: chain entanglement. Chain entanglement, which arises as polymer strands cannot pass through one another in a polymer network, is an important non-covalent stiffening mechanism for polymeric materials¹³. As entangled chains are 'mobile' in the network and allow mechanical energy to be dissipated in many chains and over long lengths, chain entanglements will stiffen but not

¹Department of Chemistry, The University of British Columbia, Vancouver, British Columbia, Canada. ²State Key Laboratory of Pharmaceutical Biotechnology, Division of Sports Medicine and Adult Reconstructive Surgery, Department of Orthopedic Surgery, Branch of National Clinical Research Center for Orthopedics, Drum Tower Hospital affiliated to Medical School of Nanjing University, Nanjing, People's Republic of China. ³National Laboratory of Solid State Microstructures, Department of Physics, Nanjing University, Nanjing, People's Republic of China. ⁴These authors contributed equally: Linglan Fu, Lan Li. ✉e-mail: hongbin@chem.ubc.ca

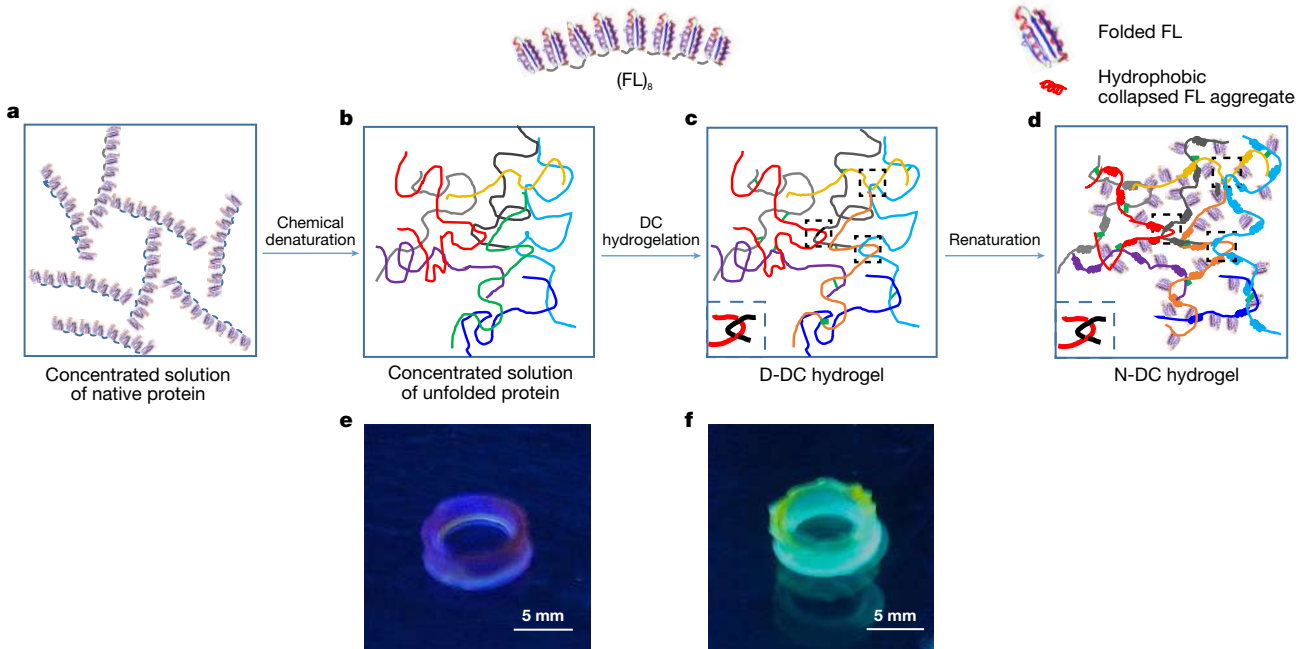


Fig. 1 | Schematics of the chain-entangled network structure of the N-DC (FL)₈ hydrogel. **a–d**, Schematics of the preparation of D-DC and N-DC (FL)₈ hydrogels. At the top are shown schematic structures of folded (FL)₈ and hydrophobic collapsed FL aggregate, as well as the three-dimensional structure of folded FL. Folded FL is an $\alpha+\beta$ protein with its β sheet packing against its two α helices. The hydrophobic collapsed FL aggregate is depicted as a spiral-shaped structure. The DC hydrogels are prepared by crosslinking unfolded proteins in their concentrated solutions. **a**, First, a concentrated solution of the native, folded elastomeric protein (FL)₈ was prepared in PBS (with a concentration of 200 mg ml⁻¹). **b**, (FL)₈ was then denatured using GdHCl and the unfolded (FL)₈ polypeptide chains, which behaved as random coils, probably overlapped with one another in the concentrated protein solution, leading to possible chain entanglements. To help visualize the entanglements, each individual (FL)₈ molecule is coloured separately in **b–d**. Upon photo-crosslinking, the unfolded protein solution was crosslinked into the D-DC

hydrogel, in which (FL)₈ remain unfolded. **c**, After crosslinking, chain entanglements were retained in the hydrogel, leading to a network of entangled polypeptide chains. Entangled chains are highlighted in dashed squares. **d**, The D-DC hydrogel was then converted to N-DC hydrogel by renaturing (FL)₈ in PBS. Upon renaturation, some FL domains refolded (as highlighted by the folded $\alpha+\beta$ structure of FL), whereas others underwent hydrophobic collapse (as indicated by the spiral-shaped aggregate structure). In the N-DC hydrogel, the chain entanglements remained (highlighted in dashed squares), making the N-DC hydrogel an entangled network of folded and hydrophobically collapsed proteins. **e**, A photograph of (FL-M23C)₈ N-DC hydrogel under UV light. The blue fluorescence was from the dityrosine crosslinking points. **f**, A photograph of a (FL-M23C)₈ N-DC hydrogel under UV light after labelling with IAEDANS. The cyan fluorescence was from the labelling of the exposed cysteine residues, and indicated that some FL domains were unfolded in the hydrogel.

embrittle the polymer network, a unique feature that has not been fully appreciated.

In muscle, titin is organized as parallel bundles²³. In soft protein hydrogels engineered from polyproteins made of tandem repeats of globular domains, no chain entanglement is present either, owing to their short length (approximately 10 nm to 40 nm)^{9,18}. Here we use the polyprotein (FL)₈, which consists of eight tandem repeats of a de novo-designed ferredoxin-like protein (FL)²³ (Fig. 1), to explore the feasibility of introducing chain entanglements into a soft protein hydrogel to significantly increase its stiffness without compromising its toughness.

FL is mechanically labile and readily unfolds at about 5 pN (ref. 18). (FL)₈ has been used to construct soft (with a Young's modulus *E* of about 16 kPa) yet highly tough protein hydrogels¹⁸, with forced unfolding of FL as a highly effective energy dissipation mechanism¹⁸. No chain entanglement is present in (FL)₈ hydrogels, as folded (FL)₈ is only about 10 nm long, despite its large molecular weight (*Mw* \approx 80 kDa).

However, unfolded (FL)₈ is about 260 nm long, equivalent to the length of polystyrene with a *Mw* \approx 170 kDa. As expected for polymers, unfolded (FL)₈ polypeptide chains overlap and probably entangle in (FL)₈ concentrated solution, as evidenced by its high viscosity²⁴ (Extended Data Fig. 1). If unfolded (FL)₈ is crosslinked from its concentrated solution, chain entanglements should be trapped within the chemically crosslinked hydrogel network.

To test this, we developed the denatured crosslinking (DC) method to construct hydrogels of unfolded (FL)₈ using the tris(bipyridine)

ruthenium(II)([Ru(bpy)₃]²⁺)-mediated photo-crosslinking strategy^{9,16,25,26}, which crosslinks two adjacent tyrosine residues into a dityrosine. First, a concentrated (200 mg ml⁻¹) solution of native (FL)₈ (Fig. 1a) was denatured using 7 M guanidine hydrochloride (GdHCl) to prepare a concentrated solution of unfolded (FL)₈ (Fig. 1b), which was then photo-crosslinked to obtain the denatured DC hydrogel (D-DC hydrogel; Fig. 1c). As a control, we constructed a denatured (FL)₈ hydrogel that is free of chain entanglements using the native crosslinking (NC) method (Extended Data Fig. 2a–c): a concentrated solution of native (FL)₈ in phosphate-buffered saline (PBS) was first crosslinked into a hydrogel, which is entanglement-free owing to the short length of native (FL)₈ (Extended Data Fig. 2b). The prepared hydrogel was then denatured in 7 M GdHCl to obtain the denatured NC hydrogel (D-NC hydrogel).

The resultant D-DC hydrogel was self-standing whereas the D-NC hydrogel collapsed onto itself (Fig. 2a). Tensile tests revealed that the D-DC hydrogel had *E* = 56 kPa, considerably higher than that of D-NC hydrogel (*E* \approx 1 kPa).

According to rubber elasticity theory¹³, $E = \frac{3\rho RT}{M_c} \left(1 - \frac{2M_c}{M_n}\right)$, where *E* is Young's modulus, ρ is the polymer density in the network, *R* is the gas constant, *T* is the absolute temperature, *M_n* is the polymer's number average *Mw*, and *M_c* is the average *Mw* of elastically effective strands. From the experimentally measured *E*, *M_c* can be determined and the total amount of effective crosslinking points in the network *N_{eff}* can be obtained: $N_{eff} = \frac{M_n}{M_c} \times n$, where *n* is the moles of the polymer in the network. We found that *N_{eff}(D-DC)* is about $1.6 \times N_{eff}(D-NC)$.

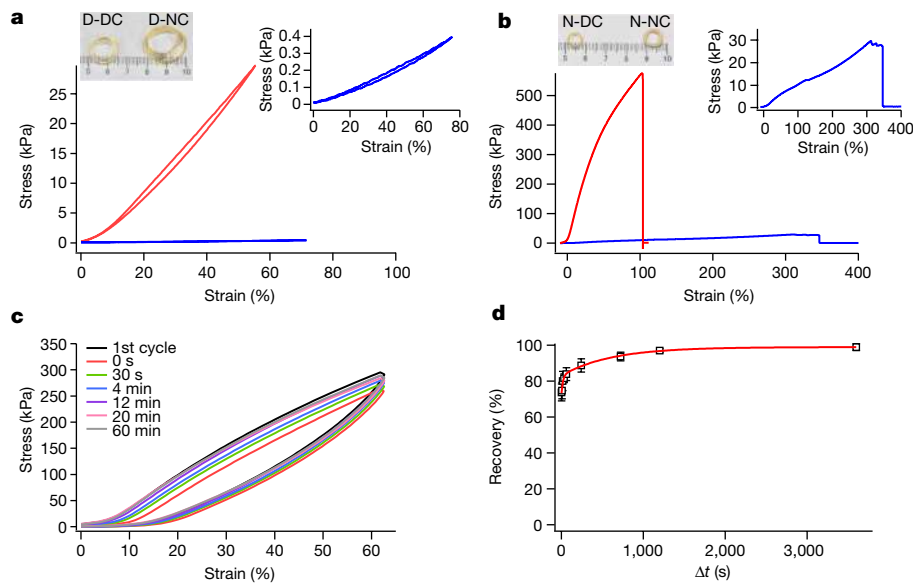


Fig. 2 | Chain entanglements enhance the stiffness of $(FL)_s$ hydrogels.

a, Stress–strain curves of D-DC (red) and D-NC (blue) $(FL)_s$ hydrogels (200 mg ml^{-1}). Right inset: a zoomed-in view of the stress–strain curve of the D-NC hydrogel. The D-DC hydrogel showed a Young’s modulus of about 50 kPa, significantly higher than that of D-NC hydrogel (about 1 kPa). Left inset: photographs of both hydrogels after being equilibrated in 7 M GdHCl. The D-DC hydrogel is self-standing and swells to a much lesser degree than the D-NC hydrogel. **b**, Stress–strain curves of N-DC (red) and N-NC (blue) $(FL)_s$ hydrogels (200 mg ml^{-1}) in PBS. Right inset: a zoomed-in view of the stress–strain curve of the N-NC hydrogel. The D-DC hydrogel had a Young’s modulus of about 0.7 MPa, significantly higher than that of the N-NC hydrogel (about 20 kPa). The N-DC hydrogel ruptured at about 100% strain. Left inset: photographs of both hydrogels equilibrated in PBS. The N-DC hydrogel is translucent, whereas the

N-NC hydrogel is opaque. **c**, Stretching–relaxation stress–strain curves of the N-DC $(FL)_s$ hydrogel show large hysteresis, indicative of large energy dissipation. The capability of the N-DC $(FL)_s$ hydrogel to dissipate energy recovered rapidly upon unloading. The hydrogel was first stretched to about 60% strain and then relaxed to zero strain. After waiting for certain time Δt , the hydrogel was subject to the stretching–relaxation cycle again. The deformation recovery can be directly observed. **d**, The kinetics of the deformation recovery in N-DC $(FL)_s$ hydrogel. Error bars correspond to s.d. ($n = 3$). About 70% of the hysteresis can be recovered rapidly within a few seconds, and the remaining 30% hysteresis can be recovered following a double-exponential kinetics. The red line is a double-exponential fit to the data, with a rate constant k_1 of $0.05 \pm 0.02 \text{ s}^{-1}$ and k_2 of $(1.7 \pm 0.3) \times 10^{-3} \text{ s}^{-1}$.

However, both D-DC and D-NC hydrogels had roughly the same number of chemical crosslinks N_{chem} (about 17% of tyrosine residues in $(FL)_s$ were crosslinked), as determined from dityrosine fluorescence (Fig. 1e and Methods). As N_{chem} and unfolded $(FL)_s$ –solvent interactions are the same for both hydrogels, the higher N_{eff} (D-DC) must arise from the entanglements of unfolded $(FL)_s$ chains in the D-DC hydrogel network.

As chain entanglements in a crosslinked network cannot be removed without breaking network strands, they will be retained in the network when unfolded proteins refold. On the basis of this feature, we renatured the D-DC hydrogel in PBS to allow FL to refold, resulting in the native DC (N-DC) hydrogel (Fig. 1d). The N-DC hydrogel deswelled markedly from its D-DC form, and changed from transparent to largely translucent, whereas the N-NC hydrogel deswelled from its D-NC form and turned opaque (Fig. 2a,b). DC and NC hydrogels can be cycled between their native and denatured states reversibly. The deswelling of the N-DC hydrogel is probably due to the refolding of some FL domains, which is accompanied by the shortening of $(FL)_s$ (from 260 nm to 10 nm), and hydrophobic collapse of FL domains that remain unfolded²⁷. Scanning electron microscopy imaging revealed that both N-DC and N-NC hydrogels show microporous structures, but the N-DC hydrogel has a significantly smaller pore size than its N-NC counterpart (Extended Data Fig. 3).

Owing to the presence of chain entanglements, it is expected that in the N-DC gel, some FL would not refold, and instead undergo hydrophobic collapse, as PBS is a poor solvent for unfolded FL. Therefore, the N-DC $(FL)_s$ hydrogel probably assumes a single network structure consisting of both folded and unfolded FL domains (Fig. 1d).

The existence of unfolded FL in the N-DC hydrogel was verified using the cysteine shotgun labelling approach (Methods), which allows for labelling of only solvent-exposed cysteine residues using

thiol-reactive fluorescent dye 5-((2-((iodoacetyl)amino)ethyl)amino)naphthalene-1-sulfonic acid (IAEDANS)²⁸. For this experiment, we used a cysteine variant FL-M23C, whose Cys23 is buried in the hydrophobic core of folded FL and can be labelled only when FL-M23C is unfolded²⁷. The N-DC $(FL\text{-M23C})_s$ hydrogels showed similar physical and mechanical properties to $(FL)_s$ (Methods). After labelling in PBS, the N-DC hydrogel showed the characteristic cyan fluorescence of IAEDANS under ultraviolet (UV) illumination (Fig. 1f). Quantitative analysis showed that $50 \pm 6\%$ ($n = 3$) of FL domains were unfolded in the N-DC hydrogel (Methods).

Highly stiff and tough N-DC hydrogels

Tensile measurements showed that the N-DC $(FL)_s$ hydrogel was much stiffer than the N-NC and D-DC hydrogels, with $E = 0.70 \pm 0.11 \text{ MPa}$ ($n = 18$) (Fig. 2b), significantly higher than that of protein-based hydrogels^{9,10,16,17,29}. The N-DC hydrogel showed good stretchability with a breaking strain of $107 \pm 14\%$, and high toughness of $250 \pm 68 \text{ kJ m}^{-3}$ (defined as the energy absorbed before fracturing). Similar mechanical properties were also observed in 10% and 15% N-DC $(FL)_s$ hydrogels, as well as 20% N-DC hydrogels of $(FL)_4$ and $(FL)_{16}$ (Extended Data Fig. 4).

Moreover, N-DC $(FL)_s$ hydrogels showed large hysteresis in the stretching–relaxation cycles, indicative of large energy dissipation, and fast recovery after unloading (Fig. 2c). After being stretched to 60% strain and then relaxed to zero, 70% of its original energy dissipation capability recovered immediately after unloading, and the remaining 30% recovered more slowly (Fig. 2d). Similar to protein hydrogels and muscle fibres^{9,18,30,31}, this high energy dissipation and fast recovery probably result from forced unfolding and subsequent refolding of a small number of FL domains in the hydrogel.

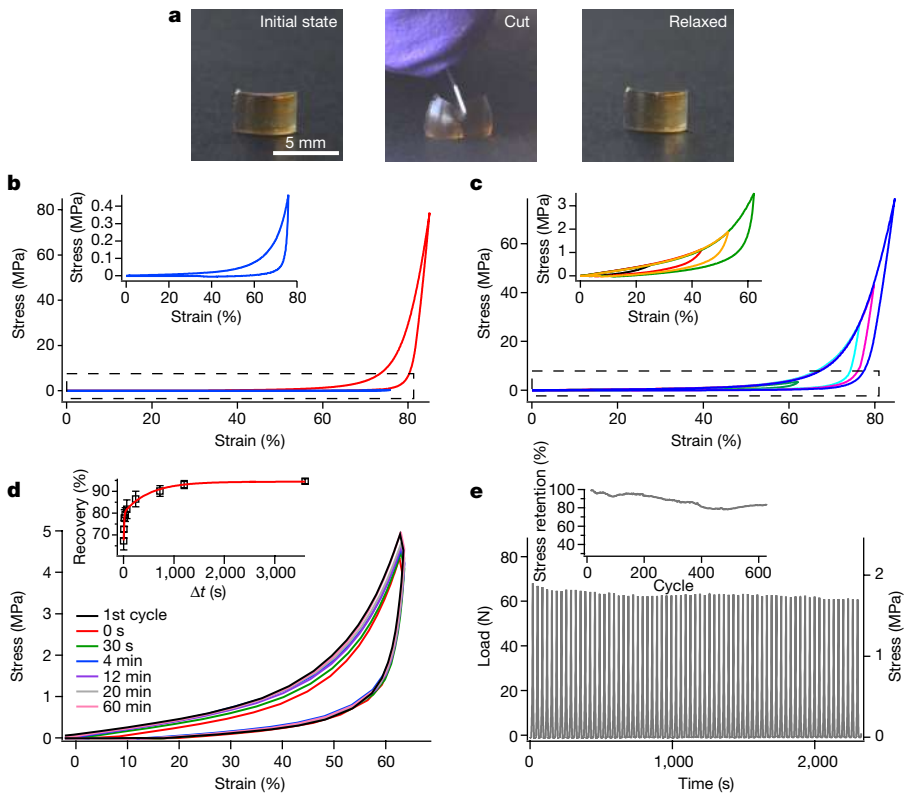


Fig. 3 | N-DC(FL)₈ hydrogels showed superb compressive mechanical properties. **a**, Photographs show that the N-DC(FL)₈ hydrogel can resist cutting with a sharp scalpel. **b**, Compressive stress–strain curves of the N-DC (red) and N-NC(FL)₈ (blue) hydrogels. Inset: zoom-in view of the stress–strain curves of the N-NC hydrogel. The N-DC hydrogel can be compressed to more than 80% strain and sustain a compressive stress of more than 70 MPa without failure. A large hysteresis was present between the loading and unloading curves, indicating that a large amount of energy was dissipated. **c**, Consecutive compression–unloading curves of the N-DC hydrogel show that the hysteresis grows with the increasing of the strain. The toughness of the hydrogel is about 3.2 MJ m^{-3} . Inset: zoom-in view of the stress–strain curves at lower strain. **d**, Consecutive compression–unloading cycles show that the deformation of the N-DC hydrogel can be recovered rapidly. Inset: the deformation recovery

kinetics of the hydrogel. About 65% of the energy dissipation capability can be recovered right after unloading, and the remaining can be recovered following a double-exponential kinetics, with k_1 of $0.10 \pm 0.02 \text{ s}^{-1}$ and k_2 of $(2.0 \pm 0.3) \times 10^{-3} \text{ s}^{-1}$. Error bars correspond to s.d. ($n = 3$). **e**, Consecutive loading–unloading curves of the N-DC(FL)₈ hydrogel at a frequency of 0.08 Hz. The pulling speed was 20 mm min^{-1} . In each cycle, the hydrogel was stretched to 50% strain and subsequently relaxed to zero strain. Inset: retention of stress at 50% strain as a function of the compression–unloading cycle. The retention is defined as 100% for the first cycle. After 600 cycles, the hydrogel showed little fatigue, and the stress of the hydrogel at 50% strain retained about 83% of the original stress in the first cycle. All the measurements were carried out using 20% N-DC(FL)₈ hydrogels.

Superb compressive properties

N-DC(FL)₈ hydrogels exhibited even more striking compressive properties (Fig. 3). The N-DC(FL)₈ hydrogel is super-tough and can resist slicing with a sharp scalpel, despite containing about 60% water (Fig. 3a). Compression tests showed that N-DC hydrogels had a compressive modulus Y of about 1.7 MPa at 10–20% strain, significantly higher than that of N-NC hydrogels (about 50 kPa) (Fig. 3b). Strikingly, the N-DC(FL)₈ hydrogel could be compressed to more than 80% strain and sustain a stress as high as 75 MPa without fracture (Fig. 3b). The N-DC(FL)₈ hydrogel shows an average compressive strength of $68 \pm 12 \text{ MPa}$ ($n = 7$) and an average failure strain of $82 \pm 3\%$. The failure was not brittle, and a small crack often started to appear in the hydrogel at failure (Extended Data Fig. 5a).

These results showed the ultrahigh compressive modulus, strength and toughness of the N-DC(FL)₈ hydrogel. The compressive modulus (1.7 MPa) and strength (68 MPa) of the N-DC(FL)₈ hydrogel are among the highest achieved for hydrogels (Supplementary Table 2), and compare favourably with those of articular cartilage (0.2–10 MPa in modulus and 10–50 MPa in strength)^{4,7,20}. For comparison, super-tough double-network polymer hydrogels show $Y = 0.3\text{--}3.9 \text{ MPa}$ and a strength of <20 MPa (refs. 32,33), poly(vinyl alcohol)/nanofibre

composite hydrogel shows $Y = 1\text{--}4 \text{ MPa}$ and a strength of 6–26 MPa (ref. 34), and cojoined network chitosan–gelatin phytate hydrogel shows $Y = 6.6 \text{ MPa}$ and a strength of 64 MPa (ref. 35).

Compression–unloading cycles show a large hysteresis thus energy dissipation, which increases with strain (Fig. 3c). At 80% strain, the hydrogel exhibited a toughness of $3.2 \pm 0.6 \text{ MJ m}^{-3}$ ($n = 7$). Moreover, N-DC hydrogels showed excellent recovery properties upon unloading (Fig. 3d, Extended Data Fig. 5b,c and Supplementary Video 1). At lower strains (<40%), the hydrogel recovered its dimension immediately after unloading. At larger strains (>60%), about 65% of the original energy dissipation capability recovered immediately after unloading, and the remaining 35% recovered within an hour (Fig. 3d). Furthermore, the hydrogel did not show significant fatigue on a timescale of 2 h after 600 consecutive loading–unloading cycles at a frequency of up to 0.67 Hz and a final strain of 60% (Fig. 3e and Extended Data Fig. 5d,e).

Collectively, these results revealed that N-DC(FL)₈ hydrogels are mechanically stiff and tough, can recover from deformation rapidly, and do not show much fatigue in both tensile and compression tests. These exceptional mechanical properties and their unique integration in one material are rare for protein hydrogels, and compare favourably with those of polymer hydrogels with special network structures (Supplementary Table 2). These properties are close to those of articular cartilage, making the

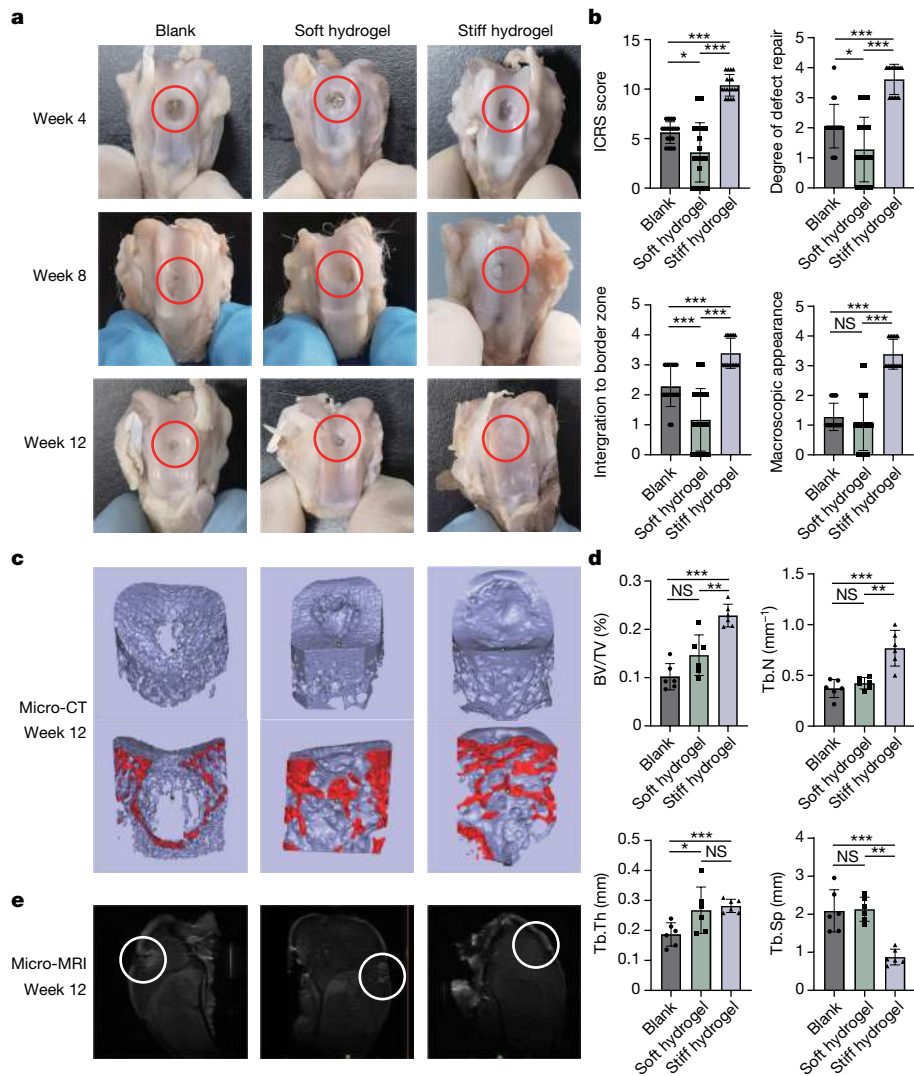


Fig. 4 | Stiff hydrogel group shows good repair efficacy of subchondral bone and cartilage at 12 weeks post-implantation. Stiff hydrogel: N-DC FLRGD hydrogel ($\gamma = 0.21 \text{ MPa}$); soft hydrogel: N-NC FLRGD/gelatin hydrogel ($\gamma = 35 \text{ kPa}$). **a**, General view of the cartilage and subchondral defect regions of the three groups at three time points post-implantation. **b**, Total ICRS score and detail scoring content of ICRS score system at 12 weeks post-implantation. Data are presented as mean \pm s.d. ($n = 6$). **c**, Micro-CT analysis shows improved subchondral bone repair in the hydrogel group at 12 weeks post-implantation. Obvious newly born bony tissue was observed in the stiff hydrogel group, and the structure of the regenerated bone was similar to the surrounding tissue. In the blank and soft hydrogel groups, a cavity existed in the defect region. **d**, Quantitative micro-CT analysis. The hydrogel group showed a higher bone volume/total volume (BV/TV) and trabecular number (Tb.N), indicating that

significant osteogenesis occurred at the hydrogel-treated region. The blank and soft hydrogel groups had a higher trabecular separation (Tb.Sp), indicative of the existence of notable bone resorption. Data are presented as mean \pm s.d. ($n = 6$). **e**, Micro-MRI analysis. In the stiff hydrogel group, a consecutive high-brightness structure in the cartilage defect region can be observed, which is similar to the surrounding cartilage tissue. The tissue below cartilage is low contrast with a relatively complete structure, similar to the surrounding bony tissue. In the blank and soft hydrogel groups, an apparent defect can be found in the cartilage and subchondral bone. The regenerated tissue in the bony region is high brightness and a distinct boundary with surrounding tissue can be observed. The untreated defect (blank) served as a control group. * $P < 0.05$; ** $P < 0.01$; *** $P < 0.001$; NS, not significant.

N-DC (FL)₈ hydrogel a cartilage-like biomaterial. It should be noted that other than mechanical properties, this material does not mimic cartilage's other properties, such as spatial structuring and transport properties.

The N-DC hydrogelation method is general

The outstanding mechanical properties of N-DC (FL)₈ hydrogels probably result from a combination of several factors, including chain entanglement, a hydrogel network consisting of both folded and hydrophobically collapsed FL, and the forced unfolding and refolding of FL. Among them, chain entanglement is essential in enhancing hydrogel stiffness without compromising toughness. Different from chemical crosslinks, chain entanglements are 'mobile' in the network, and

allow for energy dissipation in many chains, preventing hydrogels from getting brittle while being stiffened. This feat cannot be achieved by increasing chemical crosslinking density only. As chain entanglements are frequently present in concentrated solutions of unfolded proteins, this N-DC protein hydrogelation method is general. Stiff and tough N-DC protein hydrogels are engineered from a variety of elastomeric proteins, ranging from all- α proteins to $\alpha+\beta$ proteins. These hydrogels all showed significantly enhanced tensile and compressive stiffness over their N-NC counterparts. This method is also compatible with different crosslinking chemistry. For example, using disulfide crosslinking (oxidation by either oxygen (O_2) or hydrogen peroxide (H_2O_2)), we successfully prepared stiff and tough N-DC (FL-M23C)₈ hydrogels (Methods).

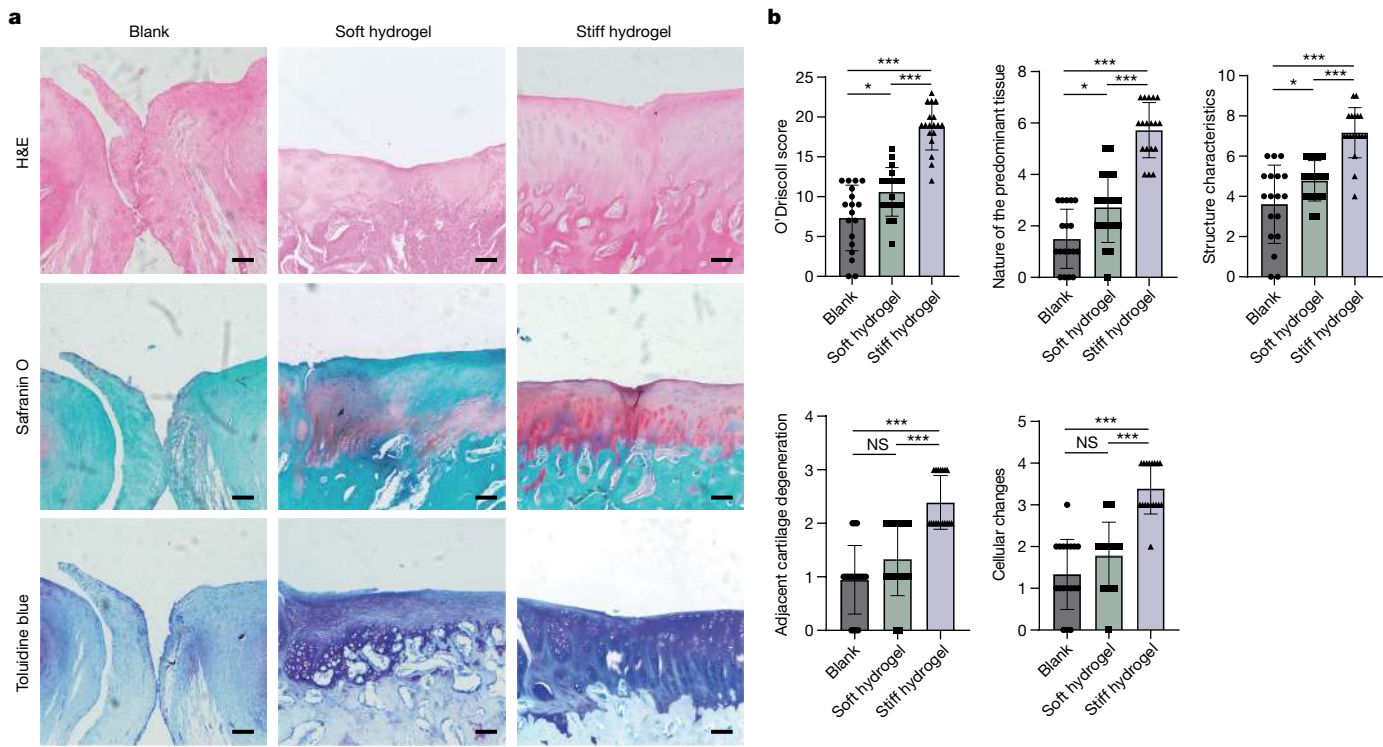


Fig. 5 | Histology analysis shows significantly improved subchondral bone and cartilage repair in the stiff hydrogel group at 12 weeks post-implantation. Stiff hydrogel: N-DC FLRGD hydrogel ($Y = 0.21 \text{ MPa}$); soft hydrogel: N-NC FLRGD/gelatin hydrogel ($Y = 35 \text{ kPa}$). **a**, Histological analysis of cartilage and subchondral bone regeneration. Scale bars, $100 \mu\text{m}$. The cellular arrangement and structural integrity in the stiff hydrogel group was similar to the natural

bone and cartilage tissues. The extracellular matrix (ECM) staining in the stiff hydrogel-treated group was also similar to that in the natural tissue. In contrast, noticeable ECM loss and irregular structure can be observed in the blank and soft hydrogel groups. **b**, Total O'Driscoll score, and detail scoring content of the O'Driscoll score system. Data are presented as mean \pm s.d. ($n = 6$). * $P < 0.05$; ** $P < 0.01$; *** $P < 0.001$; NS, not significant.

It is worth noting that chain entanglements and a hybrid protein network comprising both folded and hydrophobically collapsed proteins are required to achieve high stiffness and toughness for N-DC hydrogels. Missing either leads to the loss of high stiffness or both high stiffness and toughness (Methods). For example, gelatin lacks a folded globular structure and its N-DC and N-NC hydrogels are soft (with a similar E of about 10 kPa). Moreover, globular protein itself and the presence of unstructured protein sequences (such as resilin) may modulate the stiffness and toughness of the engineered N-DC hydrogels (Methods), thus enabling fine-tuning of the mechanical properties of engineered stiff N-DC hydrogels (with E ranging from 0.18 MPa to 0.70 MPa , and Y ranging from 0.21 MPa to 1.70 MPa ; Extended Data Table 1).

Potential biomedical applications

The mechanical properties of these stiff and tough N-DC hydrogels provide opportunities for potential biomedical applications that cannot be fulfilled by existing soft protein hydrogels, such as the repair of osteochondral defects.

Mechanical properties of matrices, such as stiffness, are important physical cues that regulate cell differentiation, tissue development and regeneration^{36,37}. Engineering biomechanically compatible microenvironments is important for tissue engineering. Repair of osteochondral defects³⁸, which involves repairing lesions of both articular cartilage and the underlying subchondral bone^{39,40}, is a major challenge. As no protein-based scaffolds with mechanical properties close to those of cartilage are available, there exists an unmet need in engineering biocompatible and biomechanically compatible scaffolds for the repair of osteochondral defects. Here we tested the potential of stiff and tough N-DC hydrogels for addressing this need.

For this, we engineered N-DC Fn-(Cys-FL)₄-RGD-(Cys-FL)₄-RGD hydrogel (for short, FLRGD), where Fn is the TNfn3 domain of the cell adhesion protein tenascin-C⁴¹, RGD is a 17-amino-acid-long sequence (TVYAVTGRGDSPASSRS) derived from fibronectin, and both contain the integrin-binding RGD (arginine-glycine-glutamate) motif. To avoid any unknown adverse biological effects of chemicals used in photo-crosslinking, we engineered the N-DC FLRGD hydrogel using disulfide crosslinking. The resultant N-DC hydrogel showed a compressive modulus of 0.21 MPa , approaching the lower end of reported moduli of cartilage⁸.

In vitro experiments showed that the N-DC FLRGD hydrogel is biocompatible, and supports cell adhesion, spreading and proliferation (Extended Data Fig. 6a,b). In addition, N-DC FLRGD hydrogels provided a stiff, osteogenic matrix to support the differentiation of mouse osteoprogenitor MC3T3-E1 cells into osteoblasts (Extended Data Fig. 6c-e), consistent with findings that stiff matrices (with a modulus $>25 \text{ kPa}$) promote osteogenic differentiation³⁶.

We then tested the N-DC FLRGD hydrogels as scaffolds for osteochondral defect repair in a rabbit model. To evaluate the effect of hydrogel stiffness on repair, we used 'naked' hydrogels in which the RGD motif is the only bioactive factor: soft N-NC FLRGD/gelatin hydrogel ($Y = 35 \text{ kPa}$), stiff N-DC FLRGD hydrogel ($Y = 0.21 \text{ MPa}$) and a blank as control (Methods).

The repair efficacy was evaluated at 4, 8 and 12 weeks post-implantation. The osteochondral defects were notably repaired in the stiff FLRGD hydrogel group at 12 weeks post-implantation (Fig. 4), but not in the control and soft FLRGD/gelatin hydrogel groups. At 12 weeks post-implantation, no hydrogel was left in the defects in the soft and stiff hydrogel groups. The defects in the blank and soft hydrogel groups were filled with irregular and depressive regenerated tissues (Fig. 4a), clearly distinguishable from the surrounding cartilage. In contrast,

Article

the regenerated tissues in the stiff hydrogel group were covered by glossy and smooth membrane, which were close to the native cartilage (Fig. 4a). The International Cartilage Repair Society (ICRS) scores confirmed these results (Fig. 4b). Micro-computerized tomography (CT) analysis revealed the success in the repair of the subchondral bone in the stiff FLRGD hydrogel group (Fig. 4c). Obvious newly born bony tissues were observed in the stiff FLRGD hydrogel group, and the structure of the regenerated bone was similar to the surrounding tissue. In contrast, a cavity existed in the defect region in the blank and soft hydrogel groups. The stiff hydrogel group showed a higher bone volume/total volume (BV/TV), trabecular number (Tb.N) and trabecular thickness (Tb.Th) (Fig. 4d), indicative of significant osteogenesis at the hydrogel-treated region. In contrast, the control group had higher trabecular separation (Tb.Sp), indicative of notable bone resorption. Micro-magnetic resonance imaging (MRI) analysis revealed similar trends (Fig. 4e). Histological results (Fig. 5a) showed that the defect of bone and cartilage in the stiff hydrogel group were filled by regenerated tissues that were uniform and smooth, and showed vertical arrangement of chondrocytes as native cartilage. In contrast, an obvious gap and cavity were observed in the blank and soft hydrogel groups. The extracellular matrix of the regenerated region showed clear regeneration of hyaline cartilage and active production of glycosaminoglycan. Overall, the stiff FLRGD hydrogel group showed higher scores in total O'Driscoll evaluation and all the detail items (Fig. 5b). Moreover, the degree of repair in the stiff FLRGD hydrogel group showed a clear progress with time, whereas the blank control and soft hydrogel group did not (Extended Data Fig. 7). This result is consistent with the time course of tissue remodelling and regeneration.

As the soft and stiff FLRGD hydrogels have similar chemical compositions but different stiffness, the superior repair efficacy achieved using the stiff N-DC FLRGD hydrogel can be reasonably attributed to the higher stiffness of the N-DC FLRGD hydrogels. It is likely that the higher stiffness, which is biomechanically more compatible with osteochondral bone and cartilage tissues, provides a suitable physical cue that is required for the effective regeneration of osteochondral bone and cartilage tissues. This finding is consistent with the findings that double-network hydrogels with moduli of 0.2 MPa promoted the regeneration of hyaline cartilage^{42,43}, highlighting the importance of improving scaffolds' biomechanical compatibility on the regeneration of cartilage. Although the detailed regeneration mechanism is unknown, it is likely that the regeneration involves the mesenchymal stem cells released from osteochondral bone marrow³⁸ (Methods). In addition, the N-DC FLRGD hydrogel showed excellent *in vivo* biocompatibility: no immunological rejection, synovial proliferation or pathological organ changes were observed in animals (Extended Data Fig. 8). Taken together, these results indicate that hydrogel scaffolds with a suitable high stiffness enhance the biomechanical compatibility of the hydrogel scaffold and improve the repair efficacy of osteochondral defects.

It is worth noting that using the highly stiff (FL-M23C)₈-Fn hydrogels ($\gamma = 0.83$ MPa) did not achieve good repair efficacy, despite its much higher stiffness (Extended Data Fig. 9). This outcome probably resulted from the much slower degradation kinetics of the highly stiff (FL-M23C)₈-Fn hydrogel *in vivo*, which in turn created a mismatch between tissue regeneration and scaffold degradation. This result highlights the complexity of cartilage regeneration, and the necessity in optimizing biomechanical cues with other biochemical and biophysical factors simultaneously for designing hydrogel scaffolds for successful repair of osteochondral defects.

Discussion

Stiff tissues often integrate seemingly mutually incompatible mechanical properties¹. Mimicking such properties using synthetic hydrogels is challenging, as optimizing one property is often at the expense of another. To resolve the incompatibility between high stiffness and high

toughness, polymer hydrogels of designed network structures, such as double-network^{32,33}, cojoined network³⁵ and slide-ring^{44,45}, and polymer composite hydrogels have been developed^{32,33,35,44–48}. Sacrificial bonds and/or a weak secondary network that can be ruptured are used for energy dissipation^{33,49,50}. Although high stiffness and high toughness were achieved in some hydrogels, slow recovery is often present, owing to the irreversible rupture of sacrificial bonds and/or slow dynamics of weak secondary networks. Proteins are attractive building blocks to construct biomaterials, but protein hydrogels are generally soft and incapable of mimicking stiff tissues (Supplementary Table 2). Here we demonstrated an N-DC hydrogelation approach to engineer stiff and tough protein hydrogels. The key to this approach is to introduce chain entanglements into the network of folded globular proteins to resolve the incompatibility between stiffness and toughness. On the one hand, chain entanglement enhances the hydrogels' stiffness without embrittling the network. On the other hand, forced unfolding of globular proteins allows for efficient energy dissipation, and refolding entails fast recovery. These effects synergistically allow the integration of high stiffness, high toughness, fast recovery and high compressive strength into protein hydrogels. Our results demonstrate the feasibility of using the same elastomeric proteins to engineer both soft and stiff protein biomaterials via the NC and DC hydrogelation strategies, thus significantly expanding the range of mechanical properties that protein hydrogels can achieve. Given the generality of this approach, the richness of potential protein building blocks, the range of mechanical properties that can be achieved, and potential applications of stiff and tough protein hydrogels in biomedical engineering, our study opens an exciting area for further systematic exploration.

Online content

Any methods, additional references, Nature Portfolio reporting summaries, source data, extended data, supplementary information, acknowledgements, peer review information; details of author contributions and competing interests; and statements of data and code availability are available at <https://doi.org/10.1038/s41586-023-06037-0>.

1. Wainwright, S. A., Biggs, W. D., Currey, J. D. & Gosline, J. M. *Mechanical Design in Organisms* (Princeton Univ. Press, 1982).
2. Higuchi, H. Viscoelasticity and function of connectin/titin filaments in skinned muscle fibers. *Adv. Biophys.* **33**, 159–171 (1996).
3. Linke, W. A., Popov, V. I. & Pollack, G. H. Passive and active tension in single cardiac myofibrils. *Biophys. J.* **67**, 782–792 (1994).
4. Hayes, W. C. & Mockros, L. F. Viscoelastic properties of human articular cartilage. *J. Appl. Physiol.* **31**, 562–568 (1971).
5. Temple, D. K., Cederlund, A. A., Lawless, B. M., Aspden, R. M. & Espino, D. M. Viscoelastic properties of human and bovine articular cartilage: a comparison of frequency-dependent trends. *BMC Musculoskelet. Disord.* **17**, 419 (2016).
6. Williamson, A. K., Chen, A. C., Masuda, K., Thonar, E. J. & Sah, R. L. Tensile mechanical properties of bovine articular cartilage: variations with growth and relationships to collagen network components. *J. Orthop. Res.* **21**, 872–880 (2003).
7. Kerin, A. J., Wisnom, M. R. & Adams, M. A. The compressive strength of articular cartilage. *Proc. Inst. Mech. Eng. H* **212**, 273–280 (1998).
8. Almarza, A. J. & Athanasiou, K. A. Design characteristics for the tissue engineering of cartilaginous tissues. *Annu. Biomed. Eng.* **32**, 2–17 (2004).
9. Lv, S. et al. Designed biomaterials to mimic the mechanical properties of muscles. *Nature* **465**, 69–73 (2010).
10. Wu, J. et al. Rationally designed synthetic protein hydrogels with predictable mechanical properties. *Nat. Commun.* **9**, 620 (2018).
11. Khouri, L. R., Shmilovich, N. J. & Popa, K. I. Study of biomechanical properties of protein-based hydrogels using force-clamp rheometry. *Macromolecules* **51**, 1441–1452 (2018).
12. Jiang, Y. & Tuan, R. S. Origin and function of cartilage stem/progenitor cells in osteoarthritis. *Nat. Rev. Rheumatol.* **11**, 206–212 (2015).
13. Treloar, L. R. G. *The Physics of Rubber Elasticity* (Oxford Univ. Press, 1975).
14. Gosline, J. et al. Elastic proteins: biological roles and mechanical properties. *Phil. Trans. R. Soc. Lond. B* **357**, 121–132 (2002).
15. Li, Y., Xue, B. & Cao, Y. Synthetic protein hydrogels. *ACS Macro Lett.* **9**, 512–524 (2020).
16. Elvin, C. M. et al. Synthesis and properties of crosslinked recombinant pro-resilin. *Nature* **437**, 999–1002 (2005).
17. McGann, C. L., Levenson, E. A. & Kiick, K. L. Resilin-based hybrid hydrogels for cardiovascular tissue engineering. *Macromolecules* **214**, 203–213 (2013).
18. Fang, J. et al. Forced protein unfolding leads to highly elastic and tough protein hydrogels. *Nat. Commun.* **4**, 2974 (2013).

19. McCutchen, C. W. *Lubrication of Joints, The Joints and Synovial Fluid* Vol. 1, 437–483 (Academic, 1978).
20. Lu, X. L. & Mow, V. C. Biomechanics of articular cartilage and determination of material properties. *Med. Sci. Sports Exerc.* **40**, 193–199 (2008).
21. Rief, M., Gautel, M., Oesterhelt, F., Fernandez, J. M. & Gaub, H. E. Reversible unfolding of individual titin immunoglobulin domains by AFM. *Science* **276**, 1109–1112 (1997).
22. Li, H. et al. Reverse engineering of the giant muscle protein titin. *Nature* **418**, 998–1002 (2002).
23. Koga, N. et al. Principles for designing ideal protein structures. *Nature* **491**, 222–227 (2012).
24. Colby, R. H. Structure and linear viscoelasticity of flexible polymer solutions: comparison of polyelectrolyte and neutral polymer solutions. *Rhol. Acta* **49**, 425–442 (2010).
25. Fancy, D. A. & Kodadek, T. Chemistry for the analysis of protein–protein interactions: rapid and efficient cross-linking triggered by long wavelength light. *Proc. Natl Acad. Sci. USA* **96**, 6020–6024 (1999).
26. Partlow, B. P., Applegate, M. B., Omenetto, F. G. & Kaplan, D. L. Dityrosine cross-linking in designing biomaterials. *ACS Biomater. Sci. Eng.* **2**, 2108–2121 (2016).
27. Fang, J. & Li, H. A facile way to tune mechanical properties of artificial elastomeric proteins-based hydrogels. *Langmuir* **28**, 8260–8265 (2012).
28. Johnson, C. P., Tang, H. Y., Carag, C., Speicher, D. W. & Discher, D. E. Forced unfolding of proteins within cells. *Science* **317**, 663–666 (2007).
29. Partlow, B. P. et al. Highly tunable elastomeric silk biomaterials. *Adv. Funct. Mater.* **24**, 4615–4624 (2014).
30. Lei, H. et al. Stretchable hydrogels with low hysteresis and anti-fatigue fracture based on polyprotein cross-linkers. *Nat. Commun.* **11**, 4032 (2020).
31. Minajeva, A., Kulke, M., Fernandez, J. M. & Linke, W. A. Unfolding of titin domains explains the viscoelastic behavior of skeletal myofibrils. *Biophys. J.* **80**, 1442–1451 (2001).
32. Gong, J. P., Katsuyama, Y., Kurokawa, T. & Osada, Y. Double-network hydrogels with extremely high mechanical strength. *Adv. Mater.* **15**, 1155–1158 (2003).
33. Gong, J. P. Why are double network hydrogels so tough? *Soft Matter* **6**, 2583–2590 (2010).
34. Xu, L., Zhao, X., Xu, C. & Kotov, N. A. Water-rich biomimetic composites with abiotic self-organizing nanofiber network. *Adv. Mater.* **30**, 1703343 (2018).
35. Xu, L. et al. Conjoined-network rendered stiff and tough hydrogels from biogenic molecules. *Sci. Adv.* **5**, eaau3442 (2019).
36. Engler, A. J., Sen, S., Sweeney, H. L. & Discher, D. E. Matrix elasticity directs stem cell lineage specification. *Cell* **126**, 677–689 (2006).
37. Discher, D. E., Janmey, P. & Wang, Y. L. Tissue cells feel and respond to the stiffness of their substrate. *Science* **310**, 1139–1143 (2005).
38. Huey, D. J., Hu, J. C. & Athanasiou, K. A. Unlike bone, cartilage regeneration remains elusive. *Science* **338**, 917–921 (2012).
39. Hunziker, E. B. Articular cartilage repair: basic science and clinical progress. A review of the current status and prospects. *Osteoarthritis Cartilage* **10**, 432–463 (2002).
40. Hayami, T. et al. The role of subchondral bone remodeling in osteoarthritis: reduction of cartilage degeneration and prevention of osteophyte formation by alendronate in the rat anterior cruciate ligament transection model. *Arthritis Rheum.* **50**, 1193–1206 (2004).
41. Leahy, D. J., Hendrickson, W. A., Aukhil, I. & Erickson, H. P. Structure of a fibronectin type III domain from tenascin phased by MAD analysis of the selenomethionyl protein. *Science* **258**, 987–991 (1992).
42. Yokota, M. et al. Spontaneous hyaline cartilage regeneration can be induced in an osteochondral defect created in the femoral condyle using a novel double-network hydrogel. *BMC Musculoskelet. Disord.* **12**, 49 (2011).
43. Li, L. et al. Biofabrication of a biomimetic supramolecular-polymer double network hydrogel for cartilage regeneration. *Mater. Des.* **189**, 108492 (2020).
44. Okumura, K. I. K. The polyrotaxane gel: a topological gel by figure-of-eight cross-links. *Adv. Mater.* **13**, 485–487 (2001).
45. Bin Imran, A. et al. Extremely stretchable thermosensitive hydrogels by introducing slide-ring polyrotaxane cross-linkers and ionic groups into the polymer network. *Nat. Commun.* **5**, 5124 (2014).
46. Liu, J. et al. Tough supramolecular polymer networks with extreme stretchability and fast room-temperature self-healing. *Adv. Mater.* **29**, 1605325 (2017).
47. Wang, J., Lin, L., Cheng, Q. & Jiang, L. A strong bio-inspired layered PNIPAM-clay nanocomposite hydrogel. *Angew. Chem. Int. Edn* **51**, 4676–4680 (2012).
48. Sun, W. et al. Molecular engineering of metal coordination interactions for strong, tough, and fast-recovery hydrogels. *Sci. Adv.* **6**, eaaz9531 (2020).
49. Sun, J. Y. et al. Highly stretchable and tough hydrogels. *Nature* **489**, 133–136 (2012).
50. Zhao, X. Multi-scale multi-mechanism design of tough hydrogels: building dissipation into stretchy networks. *Soft Matter* **10**, 672–687 (2014).

Publisher's note Springer Nature remains neutral with regard to jurisdictional claims in published maps and institutional affiliations.

Springer Nature or its licensor (e.g. a society or other partner) holds exclusive rights to this article under a publishing agreement with the author(s) or other rightsholder(s); author self-archiving of the accepted manuscript version of this article is solely governed by the terms of such publishing agreement and applicable law.

© The Author(s), under exclusive licence to Springer Nature Limited 2023

Methods

Protein engineering

The FL domain is a redesigned variant of Di-I_5 (Protein Data Bank code 2KL8)^{18,23}. The amino acid sequence of FL is: MGEFDIFRFT DDDE QFEKVL KEMNRRARKD AGTVTYTRDG NDFEIRITGI SEQNRKELAK EVERLAKEQN ITVTYTERGS LE. The genes of the polyproteins (FL)₈, (FL-M23C)₈, (FL)₄, (FL)₁₆, Fn-(Cys-FL)₄-RGD-(Cys-FL)₄-RGD and (FL-M23C)₈-Fn were constructed following standard and well established molecular biology methods as reported previously⁹. Fn is the TNfn3 domain from human extracellular matrix protein tenascin-C, and RGD is a 17-amino-acid-residue-long sequence (TVYAVTGRGDS PASSRS) derived from cell adhesion protein fibronectin that contains the integrin-binding RGD motif. Other polyproteins, (GB1)₈, (NuG2)₈, GRG₅RG₄R, N₄RN₄RNR and (GA)₈, were constructed following the same method. Amino acid sequences of the elastomeric proteins engineered in this study are shown in Supplementary Table 1. Polyprotein genes were inserted into the vector pQE80L for protein expression in *Escherichia coli* strain DH5α. Seeding culture was allowed to grow overnight in 10 ml 2.5% Luria–Bertani broth (LB) medium containing 100 mg l⁻¹ ampicillin. The overnight culture was used to inoculate 1 l LB medium, which was grown at 37 °C and 225 rpm for 3 h to reach an optical density at a wavelength of 600 nm (OD₆₀₀) of about 0.8. Protein expression was induced with 1 mM isopropyl-1-β-D-thiogalactoside and continued at 37 °C for 4 h. The cells were collected by centrifugation at 4,000 rpm for 10 min at 4 °C and then frozen at -80 °C. For polyprotein purification, cells were thawed and resuspended in 1× PBS and lysed by incubation with 1 mg ml⁻¹ lysozyme for 30 min. Nucleic acids were removed by adding 0.1 mg ml⁻¹ of both DNase and RNase. The supernatant with soluble protein was collected after centrifuging the cell mixture at 12,000 rpm for 60 min. The soluble His₆-tagged protein was purified using a Co²⁺ affinity column. The yields of (FL)₄, (FL)₈, (FL-M23C)₈ and (FL)₁₆ are approximately 90 mg, 80 mg, 80 mg and 45 mg, respectively, per litre of bacterial culture. Purified proteins were dialysed extensively against deionized water for 2 days to remove residual sodium chloride, imidazole and phosphate. Then the protein solution was filtered and lyophilized, and stored at room temperature until use. Bovine serum albumin (BSA) lyophilized powder was purchased from Sigma-Aldrich.

Hydrogel preparation and dimension measurements

Lyophilized (FL)₈ protein was dissolved in PBS and 7 M GdHCl at a concentration of 200 mg ml⁻¹ to obtain the folded and unfolded (FL)₈ protein solutions. The viscosity of the protein solution was determined by using a TA Instruments Discovery HR-2 equipped with a 20-mm flat plate.

(FL)₈ protein hydrogels were prepared using two different gelation methods. The NC hydrogels were prepared in their native state by dissolving and gelating proteins in 1× PBS. After gelation, N-NC hydrogels were soaked in PBS, whereas the D-NC hydrogels were stored in 1× PBS containing 7 M GdHCl to reach swelling equilibrium. The DC hydrogels (D-DC and N-DC) were prepared by dissolving the lyophilized (FL)₈ in 7 M GdHCl for 2 h before use. The denatured protein solution was crosslinked into hydrogels and equilibrated in 7 M GdHCl to obtain D-DC hydrogels, whereas N-DC hydrogels were renatured in PBS on a rocker by changing fresh PBS 10 times over the course of 1 day until reaching equilibrium.

Gelation of (FL)₈, (FL-M23C)₈ and (FL)₁₆ were based on a photochemical crosslinking strategy described previously^{9,16,18,25}. To prepare 20% (w/v) hydrogels, lyophilized proteins (200 mg ml⁻¹) were re-dissolved in PBS (D-NC and N-NC) or 7 M GdHCl in PBS (D-DC and N-DC). A typical crosslinking reaction mixture contained 200 mg ml⁻¹ of polyprotein, 50 mM ammonium persulfate and 200 μM [Ru(bpy)₃]Cl₂. The protein mixture was cast into a custom-made plexiglass ring-shaped mould (with a dimension of: inner diameter d_{in} = 8 mm, outer diameter d_{out} = 10 mm, height h = 3 mm), and was exposed to a 200-W fibre optical white-light source placed 10 cm above the mould for 10 min at room temperature. After gelation was complete, the hydrogel sample

was carefully taken out of the mould. After the ring-shaped hydrogels were stored in the desired buffers for 3 h (N-DC gels for 24 h), the outer diameter, thickness, width and weight of all ring-shape equilibrated swollen and deswelling samples were measured before tensile tests. For compressive tests and scanning electron microscopy imaging, the hydrogels were prepared in a cylindrical shape following the same gelation procedures. The hydrogels preparation and the tensile (E) and compressive (Y) moduli measurements of (GB1)₈, (NuG2)₈, GRG₅RG₄R, N₄RN₄R, (GA)₈ and BSA followed the same procedures.

A disulfide-based oxidation method was also used to prepare DC hydrogels of Fn-(Cys-FL)₄-RGD-(Cys-FL)₄-RGD (FLRGD), (FL-M23C)₈ and (FL-M23C)₈-Fn. Briefly, 20% protein solution in 7 M GdHCl was cast into a custom-made plexiglass mould and left to stand overnight to allow air oxidation. After the gelation, the D-DC hydrogels were carefully taken out of the mould and renatured in PBS on a rocker by changing fresh PBS 10 times over the course of 1 day until reaching equilibrium.

The soft FLRGD/gelatin hydrogel was prepared using the N-hydroxysuccinimide (NHS)-N-(3-dimethylaminopropyl)-N-ethylcarbodiimide (EDC) crosslinking chemistry. An aqueous solution of FLRGD/gelatin (with a concentration of 5% FLRGD and 5% gelatin) was prepared at 40 °C, and then left to stand at room temperature for 2 h to allow gelatin to form a physically crosslinked hydrogel. The hydrogel was then chemically crosslinked in PBS using 15 mM EDC/6 mM NHS for 1 h. The resultant hydrogel was rinsed in PBS thoroughly to remove unreacted chemicals.

Before and after testing, the N-DC protein hydrogels were stored in PBS (with 0.2% sodium azide). They showed excellent long-term stability: after storage for over eight months, their physical and mechanical properties remained largely unchanged.

Tensile tests

Tensile tests were performed using an Instron-5500R tensometer with a custom-made force gauge and a 5-N load transducer. The ring-shaped hydrogel specimen was stretched and relaxed in PBS (N-DC and N-NC) or 7 M GdHCl in PBS (D-DC and D-NC) at a constant temperature (25 °C) without special preconditioning. The stress was calculated by dividing the load by the initial cross-sectional area of the hydrogel sample. Young's modulus, breaking strain and energy dissipation were measured using an extension rate of 25 mm min⁻¹. Young's modulus of the sample was measured at a strain between 10% and 15%. Toughness was determined by integrating stress-strain curves where specimens were loaded directly to failure. Energy dissipation was calculated by integrating loop area between stretching and relaxing stress-strain curves. In deformation recovery experiments, a pulling rate of 200 mm min⁻¹ was used. The same ring sample was stretched and relaxed with various time intervals. It is of note that the mechanical properties of the N-DC hydrogel do not show obvious changes in buffers containing divalent metal ions, such as 10 mM Ca²⁺ or Mg²⁺.

For technical consideration, we used ring-shaped specimens for tensile testing. Tensile testing of rings of material was conducted to minimize difficulties that arise from gripping soft materials. Because the test strains are large in these experiments, gripped material would thin substantially upon stretching, so the material would need to be clamped so tightly that it would fail at the grips. Self-adjusting pneumatic grips that automatically adjust for material thinning are designed for materials much stiffer than our polyprotein and would have the same problem of material failure or slippage. We followed previously published methods for testing arterial elastin rings⁵¹ and protein-based biomaterials⁹ to avoid these problems.

Compression tests

Uniaxial compression tests were performed on cylinder-shaped hydrogels that were swollen to equilibrium using the Instron-5500R with a 5,000-N load transducer in air at room temperature. The dimensions (height (h_0) and diameter (d_0)) of the equilibrated N-DC and N-NC (FL)₈

hydrogel samples are $h_0 = 3.0$ mm and $d_0 = 6.5$ mm for the N-DC hydrogel, and $h_0 = 5.0$ mm and $d_0 = 5.0$ mm for the N-NC hydrogel. The gel was put on the lower plate, while the upper plate approached the sample slowly until a rise in force was detected, indicating contact between the plate and the gel. The stress was calculated by dividing the load by the initial cross-sectional area of the hydrogel sample. Unless a different rate is stated, the gel was compressed and relaxed at a compression speed of 2 mm min^{-1} . No water was squeezed out of the gels during compression. The compressive modulus was measured at a strain of 10–20%. The maximum stress and strain were determined at failure points, where the first crack in the gel was observed. Energy dissipation was calculated by integrating the loop area between compressing and relaxing stress–strain curves ($n = 7$). In hysteresis recovery experiments, a compression rate of 100 mm min^{-1} was used.

Characterization of dityrosine crosslinks in hydrogels by acid hydrolysis–fluorescence method

The degree of dityrosine crosslinking in both NC and DC (FL)₈ hydrogels was characterized following a well established fluorimetry method²⁷. Dityrosine emits at a wavelength of 410 nm when excited at 315 nm (Supplementary Fig. 1a). For quantification of the dityrosine and dityrosine-like compounds generated in NC and DC (FL)₈ hydrogels, we followed a well established fluorescence standard curve method²⁷. Typically, 20% (w/v) hydrogel samples (about 25 mg) were reacted with 100 μl hydrochloric acid (6 N) in a sealed 1.5-ml centrifuge tube in a metal heat block at 105 °C for 2 h to achieve full hydrolysis of the peptide bonds. Then, 100 μl of acid hydrolysis product was transferred into a new 1.5-ml centrifuge tube and neutralized by 10 μl sodium hydroxide (5 M). Next, 100 mM Na₂CO₃–NaHCO₃ buffer (pH 9.9) was added to a final volume of 1 ml. Fluorescence spectra of the samples were measured by a Varian Cary Eclipse fluorescence spectrophotometer. According to the fluorescence-concentration standard calibration curve of dityrosine, the yield of dityrosine and dityrosine-like products in the hydrogel was then determined ($n = 8$).

Cysteine shotgun fluorescence labelling by IAEDANS and fluorescence measurements

DC and NC (FL-M23C)₈ hydrogels for cysteine shotgun labelling were prepared with the same protein concentration and gel preparation procedures as the wild-type (FL)₈. The labelling reaction was performed in the dark at room temperature for 3 h in PBS buffer (pH 7.4) containing 5 mM (tris(2-carboxyethyl)phosphine) (TCEP) and 2 mM IAEDANS. As a control, D-DC and D-NC (FL-M23C)₈ hydrogels incubated in 7 M GdHCl (containing 5 mM TCEP, pH 7.4) were also labelled using IAEDANS. Then all hydrogels were transferred to PBS buffer containing 5 mM β -mercaptoethanol to quench the reaction. To remove excess labelling dye, additional PBS buffer (containing 5 mM β -mercaptoethanol) was added, and changed 5 times over the course of 5 h until fluorescence could no longer be detected in the buffer solution.

To quantify the fluorescence intensity of IAEDANS-labelled hydrogels, we digested the hydrogels with trypsin at 37 °C for 5 h. The digestion reaction contained 5% trypsin (relative to the hydrogel weight), 25 mM ammonium bicarbonate, 10 mM calcium chloride, 1 M GdHCl and 10 mM dithiothreitol. Unlabelled (FL-M23C)₈ hydrogel was digested in the same way to serve as a negative control. After digestion, 50 μl of the digested mixture was diluted to 3 ml using PBS buffer. The fluorescence emission spectrum was measured by a Varian Cary Eclipse fluorescence spectrometer using an excitation wavelength of 336 nm and emission at 490 nm was monitored (Supplementary Fig. 1b). An IAEDANS standard calibration curve was also created, covering a linear concentration range of 0–60 μM ($n = 8$).

Swelling ratio and water content measurements

For swelling ratio and water content measurements, ring-shaped hydrogels were weighed immediately after being taken out of the mould, and

the weight was recorded as m_i . The swollen weight m_s was recorded after gently removing excess buffer from equilibrated hydrogels. To measure dry weight of the gels (m_{dry}), the hydrogels were firstly immersed in deionized water to remove extra salts, then lyophilized for 2 days and dried in an incubator at 70 °C for 1 day. The swelling ratio (r) of the hydrogels was calculated using the following formula

$$r = \frac{m_s - m_i}{m_i} \times 100\%.$$

The water content (w) was determined by the dried gel (m_{dry}) and the equilibrated gel (m_s) (measured specimens, $n = 4$)

$$w = \left(1 - \frac{m_{\text{dry}}}{m_s}\right) \times 100\%.$$

Scanning electron microscopy imaging

Twenty percent (w/v) D-NC and N-NC (FL)₈ hydrogel samples were prepared for scanning electron microscopy imaging using a Hitachi S4700 scanning electron microscope. The samples were then shock-frozen in liquid nitrogen, and quickly transferred to a freeze drier where they were lyophilized for 24 h. Lyophilized samples were then carefully fractured in liquid nitrogen and fixed on aluminium stubs. The sample surface was coated by 8 nm of gold before scanning electron microscopy measurements.

Mechanical properties of (FL-M23C)₈ hydrogels

N-DC (FM23C)₈ hydrogels can be prepared by using the photo-crosslinking method and disulfide crosslinking method. The mechanical properties of N-DC (FM23C)₈ hydrogels prepared using both methods are comparable to those of N-DC (FL)₈ hydrogels. Young's modulus is 0.89 ± 0.10 MPa ($n = 5$) and 0.52 ± 0.06 MPa ($n = 5$) for photo-crosslinked and disulfide crosslinked hydrogels, respectively.

Modulation of the stiffness of the N-DC hydrogels

We have identified two empirical experimental approaches to tune the mechanical properties of the N-DC hydrogels. The first is to choose different folded globular proteins as building blocks to construct elastomeric proteins. Different proteins will have different mechanical stability in their folded state, and different tendency to undergo hydrophobic collapse in their unfolded state in PBS. These differences will affect the stiffness and toughness of the resultant N-DC hydrogels (Extended Data Table 1). The second is to incorporate intrinsically disordered protein sequences (such as resilin) in the elastomeric proteins. The incorporation of an unstructured protein sequence between folded globular domains will increase the flexibility of the elastomeric protein. The increased flexibility appears to soften the N-DC hydrogel network, leading to reduced stiffness. For example, incorporating resilin or RGD sequence in the elastomeric proteins led to the reduction of the stiffness of the corresponding N-DC hydrogels (Extended Data Table 1). The detailed molecular mechanisms underlying these empirical approaches remain to be elucidated in our future work. Nonetheless, these approaches offer the possibility to fine-tune the high stiffness of N-DC protein hydrogels (with Young's modulus in the range of 0.1 MPa to 1.1 MPa, and compression modulus in the range of 0.2 MPa to 1.7 MPa) for different applications.

Engineering soft and stiff FLRGD hydrogels for repair of osteochondral defect

To properly evaluate the role of hydrogel stiffness on the efficacy on repairing osteochondral defects, both stiff N-DC and soft N-NC hydrogels are needed. To avoid the adverse biological effects of ammonium persulfate and [Ru(bpy)₃]Cl₂ *in vivo*, we used disulfide-based crosslinking chemistry. As the cysteine residues in (FL-M23C)₈ are buried in the

Article

hydrophobic core in the folded state, it is not possible to engineer N-NC (FL-M23C)₈ hydrogels using disulfide-based crosslinking. To overcome this hurdle, we engineered FLRGD (Fn-(Cys-FL)₄-RGD-(Cys-FL)₄-RGD), in which Cys was placed between two neighbouring FL domains. The N-DC FLRGD hydrogel can be readily engineered by air or H₂O₂ oxidation. However, it was not possible to oxidize folded FLRGD into a hydrogel, possibly due to the steric hindrance of the folded protein structure that significantly limited the accessibility of Cys. Hence, we used a different crosslinking method to prepare the soft N-NC FLRGD hydrogel. We first prepared a mixed aqueous solution of FLRGD and gelatin (5% FLRGD and 5% gelatin) at 40 °C, and let the solution to cool so that gelatin can physically crosslink into a physical hydrogel. Then the physical gel was chemically crosslinked by using the NHS-EDC chemistry to obtain the N-NC FLRGD/gelatin hydrogel, which showed a compression modulus of 35 kPa. It is of note that we could not use the NHS-EDC chemistry to prepare homogeneous DC FLRGD hydrogels, as the NHS-EDC chemistry-mediated crosslinking reaction proceeded too rapidly in solution. Thus, the stiff N-DC FLRGD hydrogel (with a compression modulus of 0.21 MPa) and the soft N-NC FLRGD/gelatin hydrogel (with a compression modulus of 35 kPa) serve as a pair of hydrogels with similar chemical compositions but significantly contrasting stiffness for evaluating the effect of stiffness on the repair of osteochondral defects.

It is of note that gelatin is denatured collagen and contains RGD motifs, and has been widely used in studies related to cartilage tissue engineering owing to its low cost, biodegradability and weak antigenicity⁵². Previous studies have shown that compared with the blank group, gelatin can promote cartilage tissue regeneration to certain extent^{53,54}. In engineering the soft FLRGD/gelatin hydrogels, the NHS-EDC-based zero-length crosslinking method was used. Thus, other than gelatin, no other chemicals were introduced into the hydrogel network. The only chemical composition difference between the stiff N-DC FLRGD and soft N-NC FLRGD/gelatin hydrogels is gelatin. Incorporating gelatin only in the soft hydrogel group (FLRGD/gelatin) but not in the stiff hydrogel group (FLRGD) ensures that any possible repair of osteochondral defects in the stiff FLRGD group cannot be attributed to beneficial effect of gelatin.

Cytotoxicity assay

N-DC FLRGD hydrogels were prepared into a disk shape (8 mm in diameter and 1 mm in height) by air oxygen oxidation overnight, and allowed to reach swell equilibrium in PBS. After sterilization by exposure to UV irradiation, the hydrogels were put into 24-well cell culture plates and MC3T3-E1 cells were seeded on the hydrogels and wells at the density of 1 × 10⁵ per well. Growth medium, α-minimum essential medium (Gibco) supplemented with 10% fetal bovine serum (Gibco) and 1% penicillin/streptomycin solution (Gibco) were used in all incubations. After culturing for 48 h, the cells were assayed with live/dead assay kits. Briefly, the cells and samples were washed with PBS and then fixed with paraformaldehyde for 5 min. After washing with PBS again, cells were dyed with calcein AM and propidium iodide for 45 min and then observed under a laser scanning confocal microscope (Olympus 141 FV3000).

Cell differentiation

MC3T3-E1 cells were cultured on hydrogels and cell culture dishes as described above. For the gel and control groups, osteogenic differentiation medium (growth medium supplemented with 0.1 μM dexamethasone (Gibco), 50 μg ml⁻¹ ascorbic acid (Gibco) and 10 mM β-glycerophosphate (Gibco)) were used in the incubation. For the blank group, growth medium, α-minimum essential medium medium (Gibco) supplemented with 10% fetal bovine serum (Gibco) and 1% penicillin/streptomycin solution (Gibco) were used in the incubation. After culturing for 5 days or 10 days, the cells were fixed in 2% (vol/vol) paraformaldehyde for 30 min and then treated with 0.1% Triton X-100 for 15 min. After blocking in 5% (wt/vol) BSA for 1 h to minimize

non-specific binding, anti-Col I (catalogue number 14695, Proteintech) or anti-RUNX2 (catalogue number ab23981, Abcam) primary antibodies diluted with antibody dilution buffer were added to the fixed cells and incubated overnight at 4 °C. Then, the primary antibody solution was decanted and the dish was immediately washed with PBS three times for five minutes each time. After being rinsed with PBST (0.5 wt% Tween-20 in PBS) 3 times, the secondary antibody (Alexa Fluor 488 donkey anti-rabbit immunoglobulin G (H + L) in PBS) was added to the dish, and the cells were incubated for 60 min at room temperature. Then, the secondary antibody was decanted, and the cells were washed with PBST 3 × 5 min. All images were obtained using a Nikon-Ti-2U fluorescence microscope.

Quantitative PCR with reverse transcription

Total RNA was isolated from the cells cultured for 5 days and 10 days with the RNA-Quick Purification Kit (Yishan Biotech) and complementary DNA was generated with a HiScriptIIQ RT SuperMix for quantitative PCR (Vazyme Biotech). Then the results were analysed using a ChamQTM SYBR Color qPCR Master Mix (Vazyme Biotech). The amplification and detection were carried out on a LightCycler 480-II (Roche). The primer sequences are listed in Supplementary Table 3. The levels of the target transcript were normalized to that of the internal reference (2^{-ΔΔCT} method). Statistical significance was determined using Student's *t*-test or one-way analysis of variance accordingly. Statistical significance was set to *P* < 0.05.

In vivo study

The animal study was carried out in compliance with the regulations and guidelines of the Ethics Committee of Drum Tower Hospital affiliated to the Medical School of Nanjing University and conducted according to the Institutional Animal Care and Use Committee (IACUC) guidelines.

A total of 36 female New Zealand white rabbits with a body weight of 2.5 kg were used in the study. For 18 animals, one knee (chosen randomly) was used as a blank control and the other was treated with highly stiff hydrogel implants. For the other 18 animals, one knee was randomly selected to implant with soft hydrogels and the other was implanted with the stiff hydrogels. A full thickness osteochondral defect with a height of 4 mm and a diameter of 5 mm was made in the centre of the trochlear groove. The defects in the hydrogel treatment groups were implanted with a hydrogel cylinder, and the defects in the control group remained blank. Cefuroxime sodium was injected intramuscularly for 3 days after operation to avoid infection. For each time point (weeks 4, 8 and 12 post-operation), 12 animals were randomly selected and killed to evaluate the chondrogenic and osteogenesis capacity. The major organs were obtained at each time point to evaluate the biocompatibility of the hydrogels.

Statistical design of the animal experiments

To determine the sample size of the animal studies needed for the osteochondral defect repair, we carried out a statistical analysis. Based on the standard deviation of the experimental data from our previous experiments as well as those from the literature, we found that a sample size of 6 will guarantee a statistical power greater than 80%. To minimize the number of animals used in the experiments, we chose a sample size of 6 for each experiment.

Macroscopic evaluation

The ICRS macroscopic scoring was used to assess the macroscopic appearance of the repair tissue⁵⁵. The scoring criteria are shown in Supplementary Table 4, including the defect filling, integration to native cartilage and repair tissue surface topography.

Imaging examination and histological evaluation

The collected samples were fixed in 10% formalin for 24 h before the imaging examination. The XM micro-CT system (Hiscan) and the 9.4 T

Bruker Biospec 94/20 USR micro-MRI system (Bruker) were used to perform the CT and MRI tests. Then the samples were decalcified in 15% EDTA for 28 days, embedded in paraffin and cut into 5-μm-thick sections. These sections were then stained with haematoxylin and eosin (H&E), toluidine blue and safranin O. The histological results were assessed using the O'Driscoll scoring system⁵⁶; the scoring criteria are shown in Supplementary Table 5. All sections were observed using a microscope equipped with a charge-coupled device camera (Olympus).

Statistical analysis

The macroscopic and histological results were analysed by three investigators who were blind to the groups. Unpaired Student's *t*-test was performed using SPSS 19.0 software (IBM). $P < 0.05$ was considered statistically significant. * $P < 0.05$; ** $P < 0.01$; *** $P < 0.001$.

Evaluation of immunological response of animals after hydrogel implantation

A total of 18 male Sprague Dawley rats with a body weight of 250 g were used in the test. The animals were randomly divided into three groups (six rats for each group). Gelatin was used as the negative control group owing to its good biosafety and low immunogenicity. For the gelatin and stiff hydrogel groups, the gelatin or stiff hydrogel disks with a diameter of 4 mm and a height of 1 mm were subcutaneously implanted. The blank group received the same surgical procedure and remained blank in the incision. Three rats from each group were randomly selected and killed after implantation for 48 h. The other rats were killed after implantation for 7 days. The major organs and skins were obtained to evaluate the immunological response. In addition, the blood samples were also collected to test the liver function. The results are shown in Extended Data Fig. 8. After implantation for 2 days and 7 days, no obvious change could be seen in the major organs, including heart, liver, spleen, lung and kidney. The implanted region showed a similar inflammatory reaction to the blank group. No difference was found in liver function, including alanine transaminase, aspartate transaminase, albumin, creatinine and cholesterol. In addition, no pathological changes were found at the major organs of the rabbits at all three time points (4, 8 and 12 weeks) (Extended Data Fig. 8), for simplicity, only the results at the time point of 12 weeks are shown. These results clearly demonstrate the excellent biocompatibility of the stiff FLRGD hydrogel.

Possible mechanism for cartilage regeneration

Cartilage regeneration is a complex process involving many factors³⁸. The detailed molecular mechanism underlying the cartilage regeneration promoted by the N-DC FLRGD hydrogel implants is yet to be understood. However, it is likely that it follows a similar marrow stimulation mechanism on which the microfracture and augmented microfracture strategies are based³⁸. Through microfracture, which involves subchondral bone penetration, stem cells can be released from bone marrow and form a stem cell-rich clot. The hydrogel scaffold can then help promote stem cell's adhesion, proliferation and differentiation, leading to the regeneration of bone and cartilage tissues^{38,57}. Systematic work will be needed to elucidate the mechanistic details regarding the repair by the N-DC FLRGD hydrogel.

Reporting summary

Further information on research design is available in the Nature Portfolio Reporting Summary linked to this article.

Data availability

Source data are provided with this paper.

51. Lillie, M. A., Chalmers, G. W. & Gosline, J. M. The effects of heating on the mechanical properties of arterial elastin. *Connect. Tissue Res.* **31**, 23–35 (1994).
52. Bello, A. B., Kim, D., Kim, D., Park, H. & Lee, S. H. Engineering and functionalization of gelatin biomaterials: from cell culture to medical applications. *Tissue Eng. Part B* **26**, 164–180 (2020).
53. Gao, J. et al. Cell-free bilayered porous scaffolds for osteochondral regeneration fabricated by continuous 3D-printing using nascent physical hydrogel as ink. *Adv. Healthc. Mater.* **10**, e2001404 (2021).
54. Tsai, C. C. et al. Enzyme-cross-linked gelatin hydrogel enriched with an articular cartilage extracellular matrix and human adipose-derived stem cells for hyaline cartilage regeneration of rabbits. *ACS Biomater. Sci. Eng.* **6**, 5110–5119 (2020).
55. van den Borne, M. P. et al. International Cartilage Repair Society (ICRS) and Oswestry macroscopic cartilage evaluation scores validated for use in autologous chondrocyte implantation (ACI) and microfracture. *Osteoarthritis Cartilage* **15**, 1397–1402 (2007).
56. O'Driscoll, S. W., Keeley, F. W. & Salter, R. B. Durability of regenerated articular cartilage produced by free autogenous periosteal grafts in major full-thickness defects in joint surfaces under the influence of continuous passive motion. A follow-up report at one year. *J. Bone Joint Surg. Am.* **70**, 595–606 (1988).
57. Stanish, W. D. et al. Novel scaffold-based BST-CarGel treatment results in superior cartilage repair compared with microfracture in a randomized controlled trial. *J. Bone Joint Surg. Am.* **95**, 1640–1650 (2013).
58. Cao, Y., Kuske, R. & Li, H. Direct observation of markovian behavior of the mechanical unfolding of individual proteins. *Biophys. J.* **95**, 782–788 (2008).
59. Cao, Y. & Li, H. Polyprotein of GB1 is an ideal artificial elastomeric protein. *Nat. Mater.* **6**, 109–114 (2007).
60. Khouri, L. R. & Popa, I. Chemical unfolding of protein domains induces shape change in programmed protein hydrogels. *Nat. Commun.* **10**, 5439 (2019).
61. Alexander, P. A., He, Y., Chen, Y., Orban, J. & Bryan, P. N. A minimal sequence code for switching protein structure and function. *Proc. Natl. Acad. Sci. USA* **106**, 21149–21154 (2009).
62. Leahy, D. J., Aukhil, I. & Erickson, H. P. 2.0 A crystal structure of a four-domain segment of human fibronectin encompassing the RGD loop and synergy region. *Cell* **84**, 155–164 (1996).

Acknowledgements This work is supported by the Natural Sciences and Engineering Research Council of Canada (H.L.), the National Key R&D Program of China (grant no. 2020YFA0908100) (Y.C.), the National Natural Science Foundation of China (81991514 (Q.J.) and 32271408 (L.L.)), and the Natural Science Foundation of Jiangsu Province (BK202200121 (L.L.) and BK20202013 (Q.J.)). We thank R. Shadwick for assistance with Instron tests.

Author contributions H.L. conceived the project. L.F. conceptualized the DC hydrogelation strategy and performed experiments on the engineering and characterization of hydrogels and analysed the data. Q.B. and B.X. performed some of the engineering and characterization work on hydrogels and prepared hydrogel scaffolds for *in vitro* and *in vivo* experiments. J.L. performed part of the protein engineering work. L.L., Y.C., Q.J. and H.L. designed the *in vivo* experiments. L.L. and J.J. carried out the *in vitro* and *in vivo* experiments. L.F., L.L. and H.L. wrote the initial manuscript. All authors discussed the results and contributed to the final manuscript.

Competing interests L.F. and H.L. are co-inventors on a provisional patent application (application number PCT/CA2021/051622, submitted by The University of British Columbia) covering the N-DC hydrogelation method described in this article. The other authors declare no competing interests.

Additional information

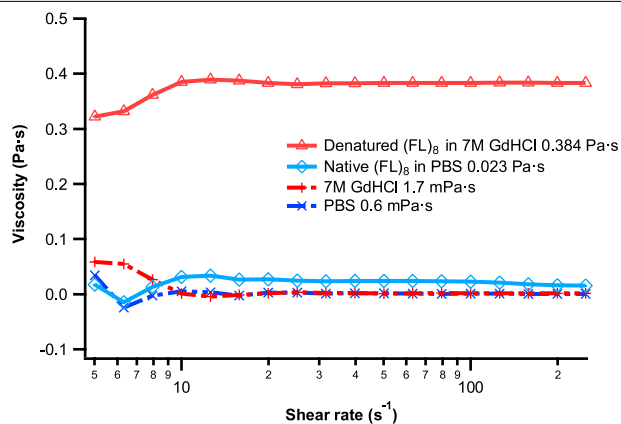
Supplementary information The online version contains supplementary material available at <https://doi.org/10.1038/s41586-023-06037-0>.

Correspondence and requests for materials should be addressed to Hongbin Li.

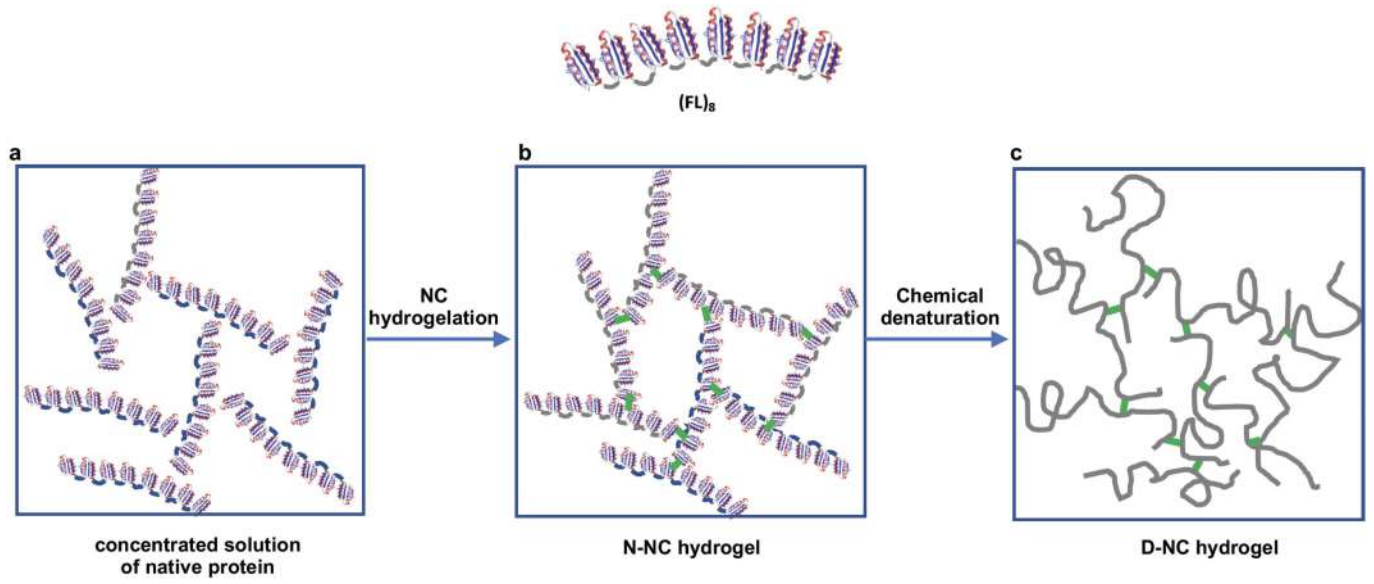
Peer review information *Nature* thanks Elliot Chaikof and the other, anonymous, reviewer(s) for their contribution to the peer review of this work. Peer reviewer reports are available.

Reprints and permissions information is available at <http://www.nature.com/reprints>.

Article



Extended Data Fig. 1 | Viscosity of native and denatured (FL)₈ protein solutions in PBS and 7M GdHCl. Denatured (FL)₈ (red triangles) displays higher viscosity than native (FL)₈ (blue diamonds).

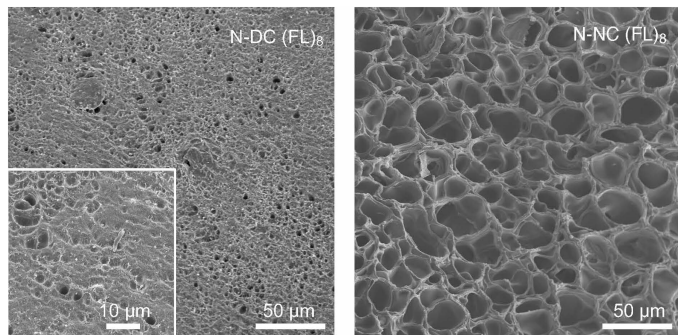


Extended Data Fig. 2 | Schematics of the NC-(FL)_s (native crosslinked)

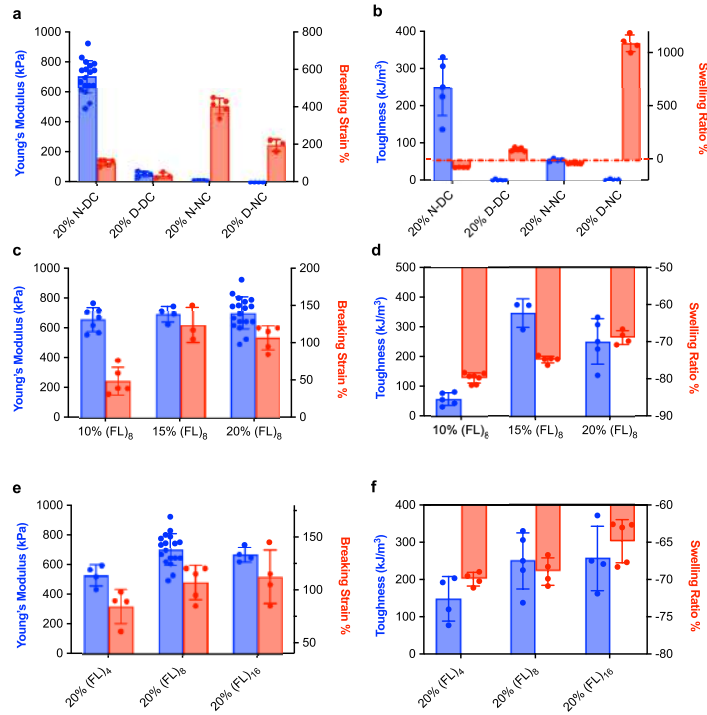
hydrogels. The elastomeric protein (FL)_s was first dissolved in PBS to a high concentration (~200 mg/mL) (a). Upon photo-crosslinking, (FL)_s were crosslinked into a hydrogel network lacking any chain entanglements, owing to the short

length of folded (FL)_s, resulting in the N-NC (native NC) hydrogel (b). When denatured in GdHCl, the (FL)_s in the hydrogel network unfold, and behave as random coils. The resultant D-NC (denatured NC) hydrogel also remains free of chain entanglements (c).

Article



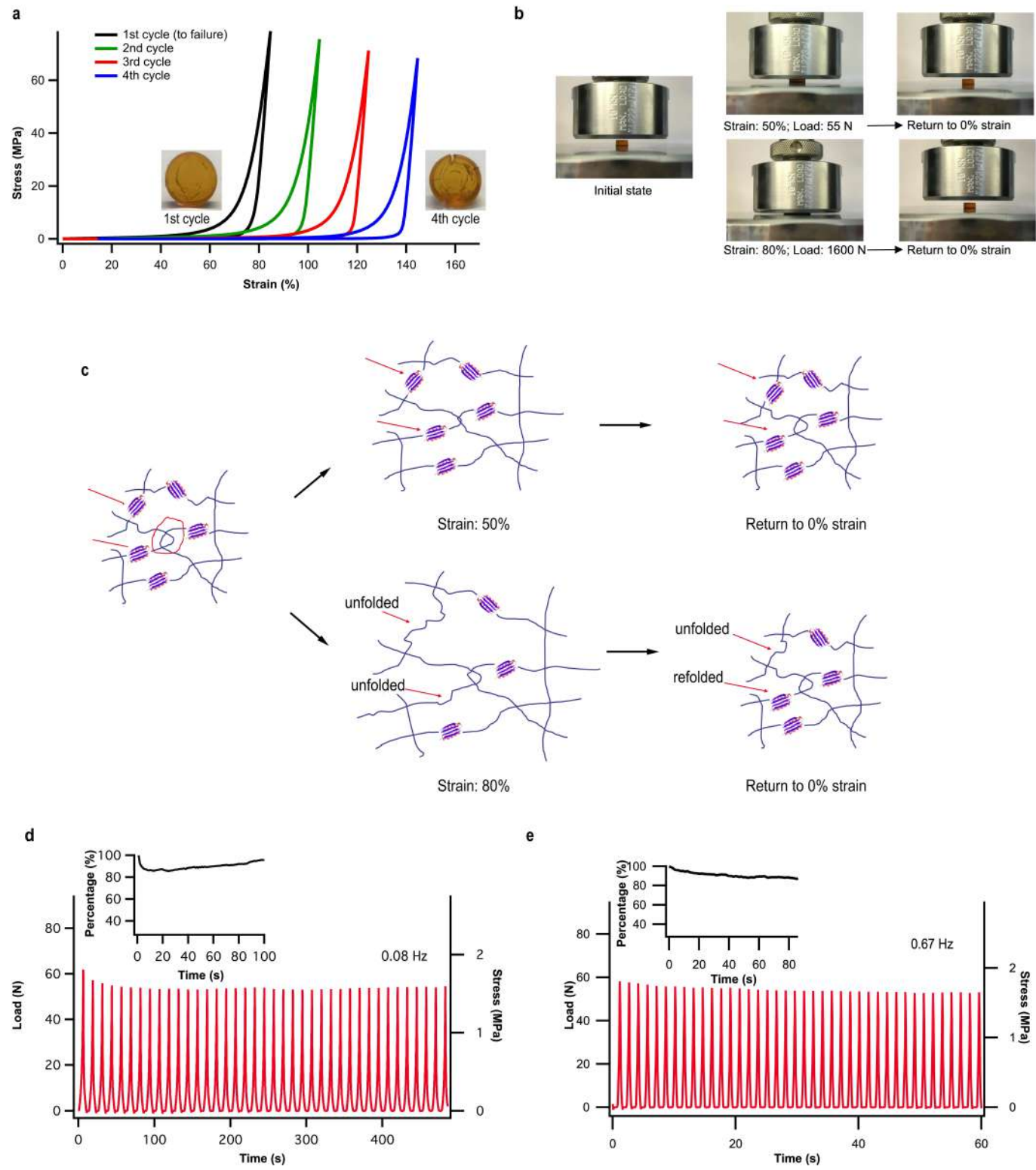
Extended Data Fig. 3 | Photographs of scanning electron microscopy imaging of N-DC and N-NC (FL)_s hydrogels. Both hydrogels have porous network structures; however, the pore size of the N-DC hydrogel (~2 μm) is significantly smaller than that of the N-NC hydrogel (~20 μm).



Extended Data Fig. 4 | Mechanical properties of N-DC and D-DC (FL)_s hydrogels in tensile testing. (a) Young's modulus and breaking strain of 20% N-DC and D-DC (FL)₈ hydrogels. (b) Toughness and swelling ratio of 20% N-DC and D-DC (FL)₈ hydrogels. It is evident that the N-DC (FL)₈ hydrogels exhibited much higher Young's modulus and higher toughness than the N-NC hydrogel. (c-d) Young's modulus/breaking strain (c) and toughness/swelling ratio (d) of N-DC (FL)₈ hydrogels at different protein concentrations. (e-f) Young's modulus/

breaking strain (e) and toughness/swelling ratio (f) of 20% N-DC hydrogels based on (FL)₄, (FL)₈ and (FL)₁₆, which consist of 4, 8 and 16 tandem repeats of FL. 20% N-DC (FL)₄ hydrogels showed similar mechanical properties as those of (FL)₈ and (FL)₁₆, suggesting that the length of unfolded (FL)₄ is sufficient for chain entanglements. The data is presented as average \pm standard deviation (ave. \pm S.D.). The number of events n ranges from 3–5 for different experiments, with the exception that n = 18 for the Young's modulus of 20% (FL)₈ N-DC hydrogel.

Article



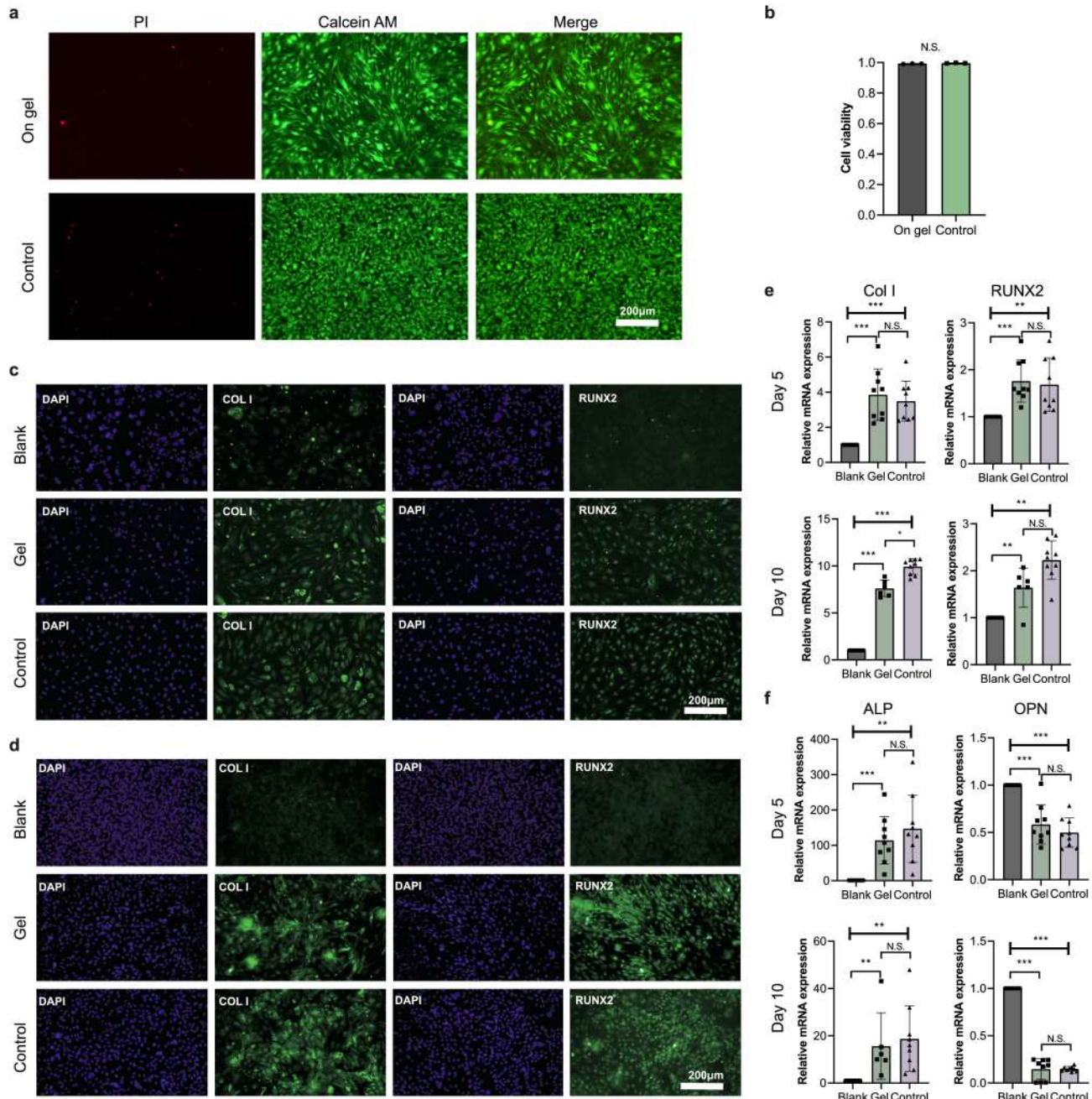
Extended Data Fig. 5 | See next page for caption.

Extended Data Fig. 5 | Compression properties of N-DC (FL)₈ hydrogels.

(**a**) Stress-strain curves of a N-DC (FL)₈ hydrogel compressed to failure. Inset shows the photographs of the hydrogel right after failure (1st cycle) and after three more consecutive compression-unloading cycles (4th cycle). Cracks were observed right after failure. Subsequent compression led to propagation of the crack, but the failure is not brittle. (**b**) Photographs of the N-DC (FL)₈ hydrogel during various stages of compression. After unloading, the hydrogel recovered its shape rapidly. (**c**) Schematics of the hydrogel network structure during compression-unloading. The structure is drawn in a highly schematic manner, and for illustration purpose only. Red circle indicates the chain entanglement, red arrows point to two folded FL domains that may undergo forced-unfolding at high strain, and then refolding after unloading. When compressed to 50%

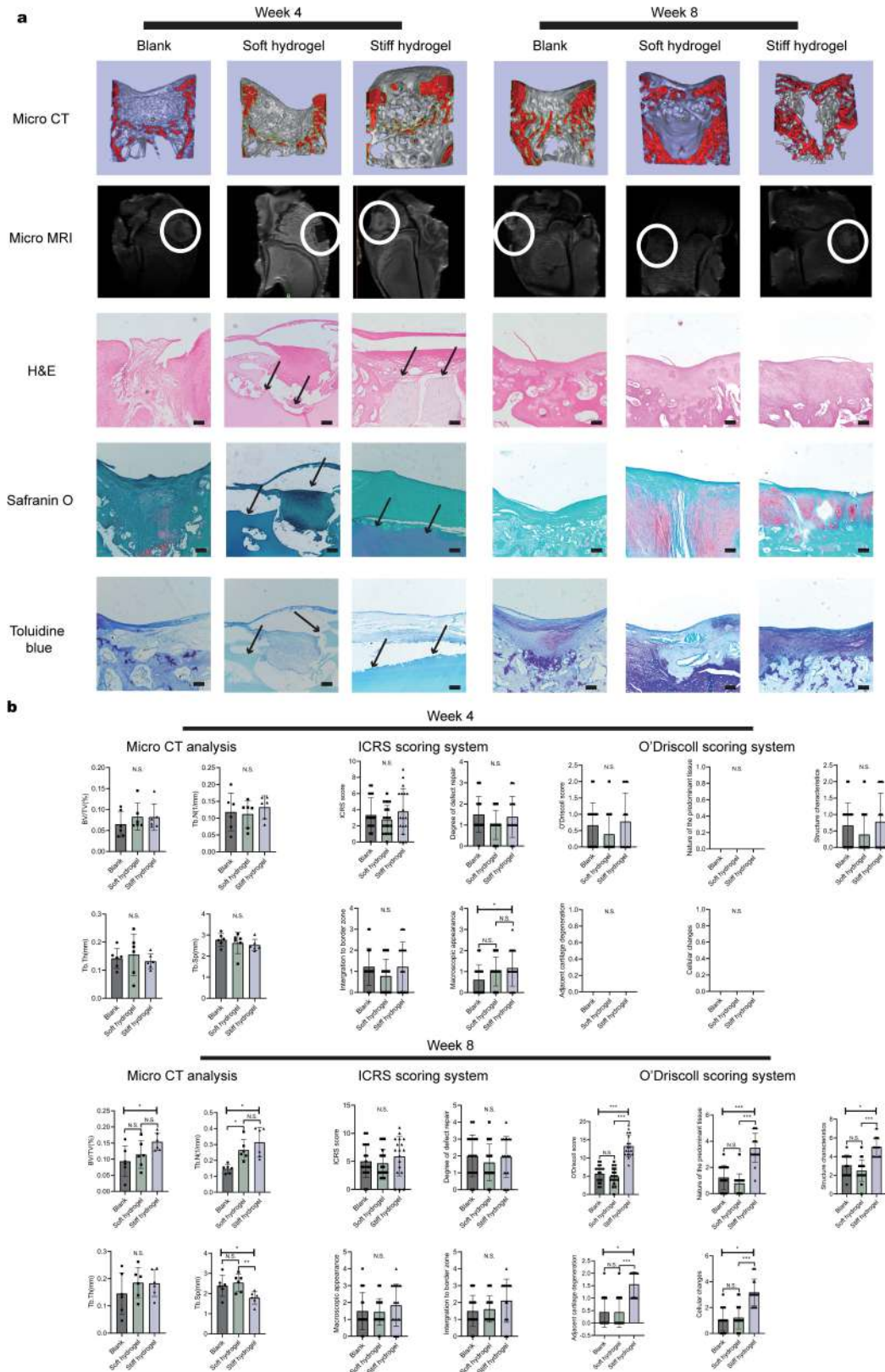
strain and then unloaded, the hydrogel can quickly recover. When compressed to 80% strain, a small number of FL domains unfold. Upon unloading, a large fraction of unfolded FL domains refolds quickly, while a small fraction refolds following a slower kinetics. For simplicity, hydrophobically collapsed FL aggregates are not shown. The force-induced unfolding of the folded FL domains help dissipate energy during loading, and upon unloading, the refolding of FL domains help the hydrogel to regain its shape and mechanical properties. (**d–e**) Consecutive compression-unloading curves of a N-DC (FL)₈ hydrogel at a frequency of 0.08 Hz (**d**) and 0.67 Hz (**e**). The loading rate was 20 mm/min in (**d**) and 200 mm/min in (**e**). The N-DC hydrogels showed limited fatigue (insets). The percentage is the peak stress of each cycle compared to the initial stress when loaded to strain of 60%.

Article



Extended Data Fig. 6 | N-DC Fn-(Cys-FL)₄-RGD-(Cys-FL)₄-RDG (FLRGD) hydrogels support cell adhesion, spreading, proliferation and differentiation of mouse osteoprogenitor MC3T3-E1 cells. (a) Epi-fluorescence images of stained cells on N-DC FLRGD hydrogels (On gel) and cell-culture dish (Control). Cells were simultaneously stained with Calcein AM dye and propidium iodide (PI) for staining live and dead cells, respectively. (b) Cell viability determined by live/dead cell staining on N-DC FLRGD hydrogels and cell-culture dish (Control). Error bars correspond to the standard deviation. (c–d) Immunostaining of MC3T3-E1 cells after cultured for 5 days (c) and 10 days (d) in blank, N-DC FLRGD hydrogel and PS culturing dish control groups. The Col I and Runx2 are specific markers for the differentiation in the direction of osteoblast. Clearly, Col I and

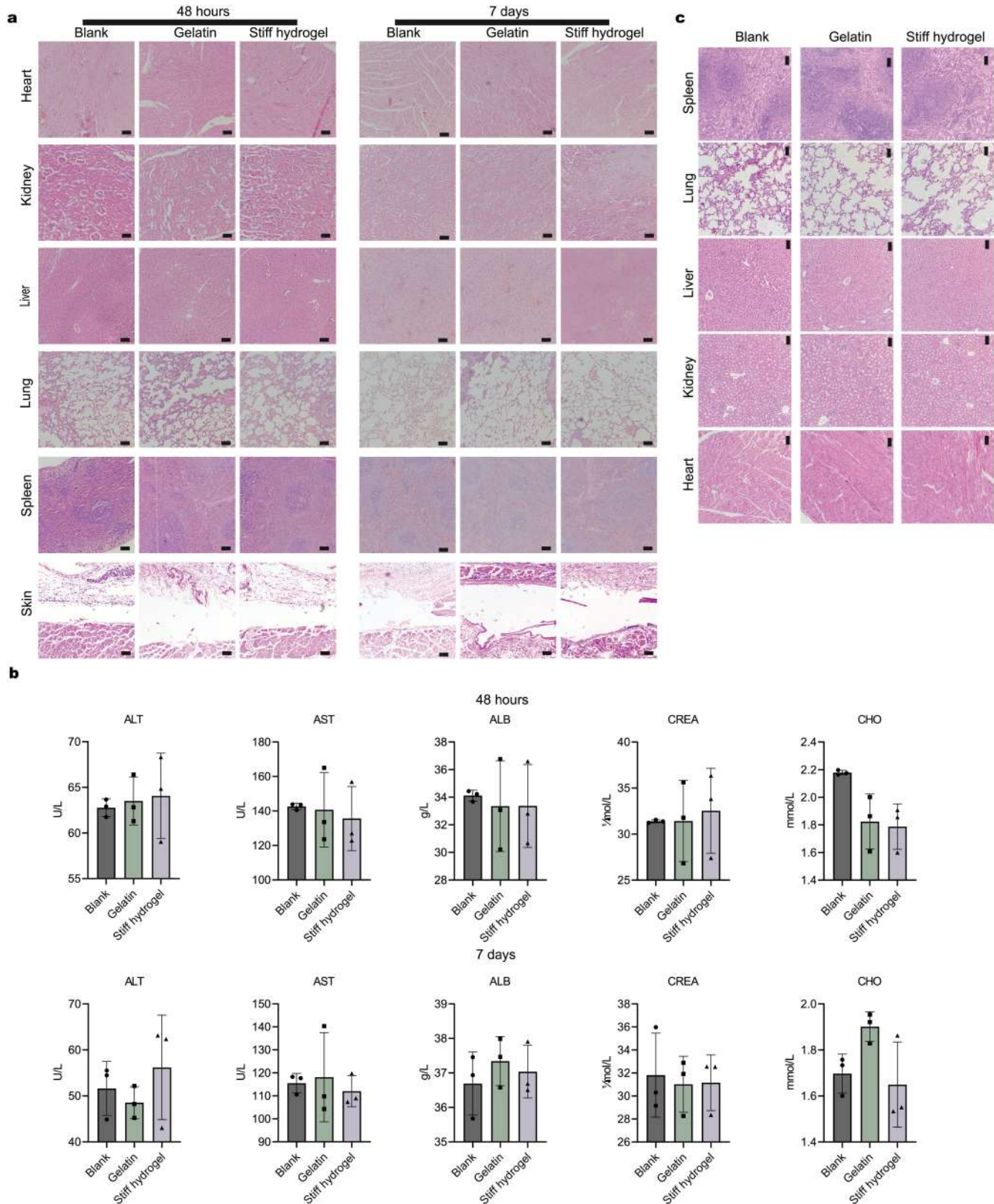
Runx2 were up-regulated in MC3T3-E1 cells cultured on N-DC-FLRGD hydrogel (Gel) and on coated cell culture dish (control) groups, while Col I and Runx2 were hardly observed in blank (uncoated cell culture dish) groups. (e and f) Expression of osteoblast differentiation-related genes (Col I, RUNX2, ALP and OPN) for MC3T3-E1 cells after cultured for 5 and 10 days. The data represent the relative mRNA levels of the target genes normalized to the levels of the reference genes and are expressed with the levels in the blank group as 1. The values represent the mean \pm s.d. Differences between groups were assessed by student's t-test; NS: p > 0.05; *: p < 0.05, **: p < 0.01, ***: p < 0.001. Cells were cultured on uncoated cell culture dish (Blank), N-DC-FLRGD hydrogel (Gel) and coated cell culture dish (Control).



Extended Data Fig. 7 | Tissue remodelling and regeneration process at different time points. (a) Imaging results and histological staining at week 4 and week 8. Scale bars: 100 µm. Arrows indicate the remaining hydrogel implants after 4 weeks of implantation. After 8 weeks of implantation, all hydrogel implants were degraded. (b) The quantitative analysis at week 4 and week 8, including Micro CT analysis, ICRS scoring system, and O'Driscoll scoring

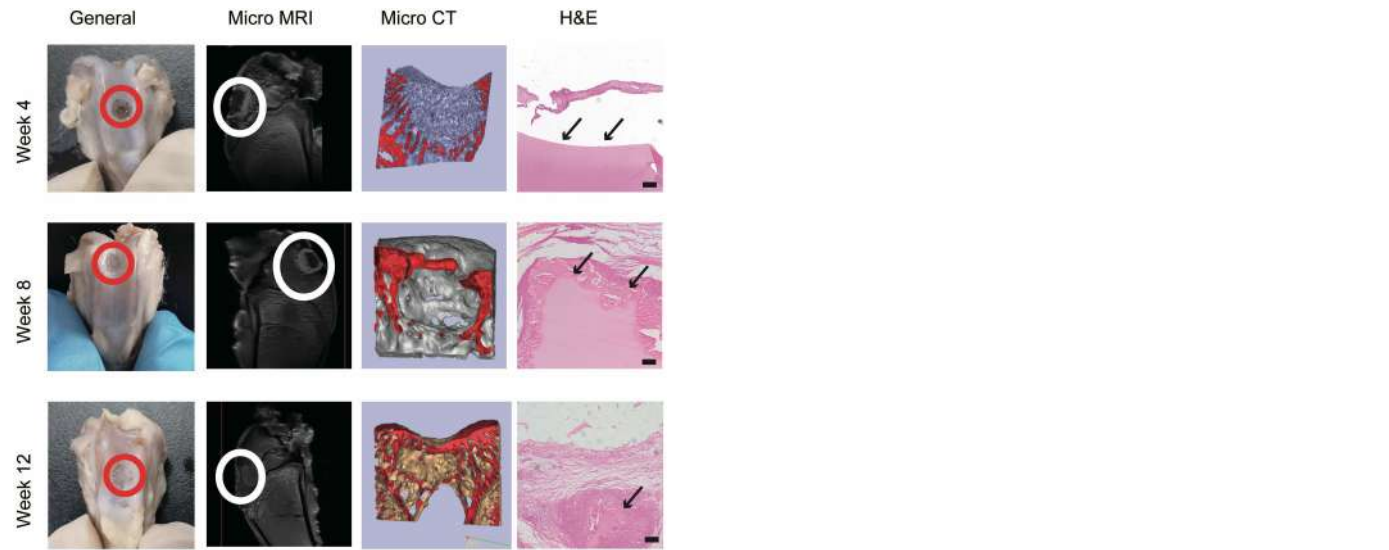
system. Data are presented as mean \pm s.d. ($n = 6$). No obvious difference was observed at week 4 among the three groups. However, the subchondral bone and cartilage in stiff hydrogel treated group exhibited better regeneration phenomenon at week 8. The statistical difference was observed in trabecular parameters and O'Driscoll scoring system. *: $p < 0.05$; **: $p < 0.01$; ***: $p < 0.001$; N.S.: not significant.

Article



Extended Data Fig. 8 | Immunological response at different time points evaluated using histology staining. (a) Histological analysis (H&E staining) of major organs and skins at time point of 48 h and 7 days. Scale bars: 100 μ m.

(b) Liver function test results at two time points. Data are presented as mean \pm s.d. ($n = 3$). (c) Histological analysis (H&E staining) of the major organs from the New Zealand rabbits after implantation for 12 weeks. Scale bars: 100 μ m.



Extended Data Fig. 9 | The repairing effect of highly stiff (FL-M23C)₈-Fn hydrogel at three time points. (a) General view of the cartilage and subchondral defects regions at three time points post implantation of the highly stiff hydrogel. Irregular tissue remained in the defect region after 12 weeks implantation. Micro MRI analysis (b) and Micro CT analysis (c) indicated that the regeneration of cartilage regeneration was scarce, and the remolding of subchondral bone was also limited. (d) Histological analysis (H&E staining) of cartilage and subchondral bone regeneration. The hydrogel implants (indicated by the arrows) can be clearly observed even after implantation for 12 weeks. Scale bars: 100 μ m.

Article

Extended Data Table 1 | Enhancement of mechanical properties via the DC hydrogelation method (E: tensile modulus; Y: compressive modulus)

	Tensile			Compression		
	N-DC hydrogel	N-NC hydrogel		N-DC hydrogel	N-NC hydrogel	
Protein	E_{N-DC} (kPa)	E_{N-NC} (kPa)	E_{N-DC}/E_{N-NC}	Y_{N-DC} (kPa)	Y_{N-NC} (kPa)	Y_{N-DC}/Y_{N-NC}
(FL) ₈	700 ± 110	15.7 ± 1.8	44	1614 ± 201	40.1 ± 2.7	40
(NuG2) ₈	620 ± 93	11.2 ± 3.3	56	1086 ± 31	55.0 ± 11	20
N ₄ RN ₄ RNR	126 ± 21	22.1 ± 2.7	5.7	592 ± 148	114 ± 25	5.2
(GB1) ₈	227 ± 30	4.8 ± 1.1	47	339 ± 36	68.3 ± 11	5.0
GRG ₅ RG ₄ R	123 ± 53	32.7 ± 4.2	3.8	220 ± 31	19.6 ± 3.9	11
BSA	236 ± 5.0	6.5 ± 0.1	36	776 ± 173	19.5 ± 3.9	40
(GA) ₈	438 ± 55	60.1 ± 9.0	7.3	1704 ± 248	95.0 ± 17	18
(FL-M23C) ₈ -Fn	380 ± 76	-		834 ± 280	-	-
FLRGD	179 ± 8.0	-	-	206 ± 15	-	-

(NuG2)₈: a polyprotein made of eight tandem repeats of the protein NuG2 (ref. 58).

(GB1)₈: a polyprotein made of eight tandem repeats of the protein GB1 (ref. 59).

GRG₅RG₄R: G represents GB1 domain, R represents the 15-residue consensus sequence of resilin (ref. 9).

NRN₄RNR: N represent NuG2 domain, R represents the 15-residue consensus sequence of resilin

BSA: bovine serum albumin (ref. 60).

(GA)₈: a polyprotein made of eight tandem repeats of the protein GA (ref. 61).

FLRGD: Fn-(Cys-FL)₄-RGD-(Cys-FL)₄-RGD, RGD represents the 17-residue sequence derived from fibronectin (ref. 62).

Reporting Summary

Nature Portfolio wishes to improve the reproducibility of the work that we publish. This form provides structure for consistency and transparency in reporting. For further information on Nature Portfolio policies, see our [Editorial Policies](#) and the [Editorial Policy Checklist](#).

Statistics

For all statistical analyses, confirm that the following items are present in the figure legend, table legend, main text, or Methods section.

n/a Confirmed

- The exact sample size (n) for each experimental group/condition, given as a discrete number and unit of measurement
- A statement on whether measurements were taken from distinct samples or whether the same sample was measured repeatedly
- The statistical test(s) used AND whether they are one- or two-sided
 - Only common tests should be described solely by name; describe more complex techniques in the Methods section.*
- A description of all covariates tested
- A description of any assumptions or corrections, such as tests of normality and adjustment for multiple comparisons
- A full description of the statistical parameters including central tendency (e.g. means) or other basic estimates (e.g. regression coefficient) AND variation (e.g. standard deviation) or associated estimates of uncertainty (e.g. confidence intervals)
- For null hypothesis testing, the test statistic (e.g. F , t , r) with confidence intervals, effect sizes, degrees of freedom and P value noted
 - Give P values as exact values whenever suitable.*
- For Bayesian analysis, information on the choice of priors and Markov chain Monte Carlo settings
- For hierarchical and complex designs, identification of the appropriate level for tests and full reporting of outcomes
- Estimates of effect sizes (e.g. Cohen's d , Pearson's r), indicating how they were calculated

Our web collection on [statistics for biologists](#) contains articles on many of the points above.

Software and code

Policy information about [availability of computer code](#)

Data collection No software was used

Data analysis No software was used

For manuscripts utilizing custom algorithms or software that are central to the research but not yet described in published literature, software must be made available to editors and reviewers. We strongly encourage code deposition in a community repository (e.g. GitHub). See the Nature Portfolio [guidelines for submitting code & software](#) for further information.

Data

Policy information about [availability of data](#)

All manuscripts must include a [data availability statement](#). This statement should provide the following information, where applicable:

- Accession codes, unique identifiers, or web links for publicly available datasets
- A description of any restrictions on data availability
- For clinical datasets or third party data, please ensure that the statement adheres to our [policy](#)

The source data underlying Figs. 2-5 is provided as Source Data files.

Field-specific reporting

Please select the one below that is the best fit for your research. If you are not sure, read the appropriate sections before making your selection.

Life sciences

Behavioural & social sciences

Ecological, evolutionary & environmental sciences

For a reference copy of the document with all sections, see nature.com/documents/nr-reporting-summary-flat.pdf

Life sciences study design

All studies must disclose on these points even when the disclosure is negative.

Sample size	The sample size of 6 was used in the hydrogel implantation studies for each group at each time point. The sample size was determined using statistical analysis. 6 samples for each group at each time point can guarantee that the statistical power is greater than 80%.
Data exclusions	Animal samples with surgical incision infection, graft abscission, joint deformity and implantation time less than 12 weeks would be excluded. According to these criterion, no data was excluded in this study.
Replication	All the in vitro experiments, including the mechanical tests and biocompatibility tests were repeated for at least 3 times on distinct samples. The surgical procedures were carried out by an experienced licensed veterinarian.
Randomization	This is not relevant for our study.
Blinding	Investigators were blinded during data collection and analysis.

Reporting for specific materials, systems and methods

We require information from authors about some types of materials, experimental systems and methods used in many studies. Here, indicate whether each material, system or method listed is relevant to your study. If you are not sure if a list item applies to your research, read the appropriate section before selecting a response.

Materials & experimental systems		Methods	
n/a	Involved in the study	n/a	Involved in the study
<input checked="" type="checkbox"/>	<input type="checkbox"/> Antibodies	<input checked="" type="checkbox"/>	<input type="checkbox"/> ChIP-seq
<input type="checkbox"/>	<input checked="" type="checkbox"/> Eukaryotic cell lines	<input checked="" type="checkbox"/>	<input type="checkbox"/> Flow cytometry
<input checked="" type="checkbox"/>	<input type="checkbox"/> Palaeontology and archaeology	<input checked="" type="checkbox"/>	<input type="checkbox"/> MRI-based neuroimaging
<input type="checkbox"/>	<input checked="" type="checkbox"/> Animals and other organisms		
<input checked="" type="checkbox"/>	<input type="checkbox"/> Human research participants		
<input checked="" type="checkbox"/>	<input type="checkbox"/> Clinical data		
<input checked="" type="checkbox"/>	<input type="checkbox"/> Dual use research of concern		

Eukaryotic cell lines

Policy information about [cell lines](#)

Cell line source(s)	MC3T3-E1 cells from Shanghai Zhong Qiao Xin Zhou Biotechnology Co.,Ltd
Authentication	Cell lines were cultured as received. No authentication was done.
Mycoplasma contamination	Cell lines were not tested for mycoplasma contamination
Commonly misidentified lines (See ICLAC register)	N/A

Animals and other organisms

Policy information about [studies involving animals](#); [ARRIVE guidelines](#) recommended for reporting animal research

Laboratory animals	Four month old female New Zealand white rabbits with a bodyweight of 2.5 kg and male SD rats with a bodyweight of 250g were used in the study.
Wild animals	The study did not involve wild animals
Field-collected samples	The study did not involve samples collected from field.

Note that full information on the approval of the study protocol must also be provided in the manuscript.